# Modeling Dissolution within Vertically Averaged Formulations

Master of Science Thesis in Applied and Computational Mathematics

## Trine Solberg Mykkeltvedt

Department of Mathematics
University of Bergen

June 2010

# Acknowledgements

First of all I would like to thank my supervisors Helge K. Dahle and Jan M. Nordbotten for their help, enthusiasm and good discussions. In parts of the process we even had fun! Also, I would like to thank Paulo Herrera for useful comments in the writing process. To all the others who have contributed in my thesis, thank you!

To all my fellow students, thank you for five unforgettable years. To Christina and Mary, thank you for welcoming me in Princeton. I would also like to thank my family and my friends for being there, and especially my nieces and nephews for making me smile. To my Erik, thank you for being there all the way.

- Finally, thank you Tassen for warming my books for seventeen years.

*Trine,*
*June 1010.*

# Abstract

In this thesis we develop a mathematical model describing the migration and trapping of $CO_2$ when injecting it in a deep saline aquifer. Both the migration and trapping processes are inherently complex, spanning multiple spatial and temporal scales. We develop a upscaled mass transfer model for these processes within vertically averaged formulations. This model is applied to a benchmark problem designed to highlight important questions about the long term fate of the injected $CO_2$.

In the developed model the effect of dissolution trapping is included. When considering dissolution trapping we distinguish between dissolution due to equilibration between mobile $CO_2$ and brine as $CO_2$ drains a region with pure brine, and dissolution due to density driven convective mixing. Using the developed model we have studied the plume migration with and without the effect of convective mixing and looked at the influence the value of the dissolution rate has on the tip velocity. Our results shows that the value of the dissolution rate has a great impact on the tip velocity. We find that the tip velocity has two characteristic values depending on the dissolution rate.

# Contents

# Outline and Motivation

Atmospheric concentrations of $CO_2$ has increased around 35% over the past 200 years [1]. This increase is largely associated with fossil fuel combustion and is expected to continue. Concerns about climate change due to this increased $CO_2$ concentration has motivated the technological approach called *carbon capture and storage* (CCS). The idea behind this is to capture the carbon before it is emitted to the atmosphere and store it in the subsurface. For this to be effective and attractive one must be able to store large amounts of carbon [4]. Currently, subsurface geological formations called *saline aquifers* are the most promising and likely site for storage of $CO_2$ [27].

**In Chapter 1** we give a short introduction to the concept of Geological storage of $CO_2$. In particular we define what is meant by a saline aquifer. Once carbon is injected to a saline aquifer, different mechanisms that leads to trapping of carbon interacts. These trapping mechanisms will be described and the different timescales they occur on will also be discussed. Furthermore, some of the challenges attached to this concept are discussed.

The feasibility of CCS depends upon our ability to inject $CO_2$ into the subsurface with a minimal risk of leakage to the atmosphere, ocean or groundwater aquifers. Therefore, governments and industry around the world are dependent on reliable estimates of how the injected carbon will migrate over time. In order to obtain those estimations we need to derive a mathematical model to represent $CO_2$ migration and solve those equations at length and time scales that are relevant to practical questions around CCS systems. Some examples of the important questions we want to answer are [7]:

- How much $CO_2$ can we store?

- How far and for how long will the injected $CO_2$ migrate?

**In Chapter 2** we introduce some of the basic concepts and definitions from

the fields of Reservoir and Fluid mechanics. Fluid flow in subsurface formations has been studied extensively within these fields. A mathematical representation of the physics of fluid flow in porous media will also be given here. These tools will be used in the other chapters to model how the injected $CO_2$ will migrate over time.

Many physical and chemical processes can affect the fate of the injected carbon. Both the migration and trapping processes are inherently complex, spanning multiple spatial and temporal scales. Appropriate models that can capture both large and small scale effects are needed. The overall mathematical description of the complete system is very complex. A usual approach to overcome this is to reduce the complexity of the system with *reasonable* assumptions. When we say reasonable assumptions we mean that the assumption is motivated from geological aspects of the storage site or our knowledge of what is a dominating feature in the process.

We know that the horizontal extent in subsurface geological formations is much larger than the vertical extent. This motivates us to assume vertical equilibrium, which reduces the problem to two spatial dimensions. As mentioned the different trapping mechanisms occur at different time scales. One can choose to only look at the influence of the processes which is assumed to dominate the first 100 years after the carbon injection stops. We will return to a discussion on these assumptions throughout the thesis.

**In Chapter 3** we give a model for the carbon migration with reduced complexity. This model only includes the trapping mechanisms that are important in the early post-injection period. This approach is similar to other works, e.g.[13, 16, 18, 23, 24], where the reduced problem is solved analytically and semi-analytically.

**In Chapter 4** we present a model that solves a reduced problem that also includes a trapping mechanism that is assumed to be important on a long temporal scale. High-resolution numerical approaches like [22, 30, 31] model the problem on the full scale and includes trapping mechanisms that dominates on later time scales. For practical problems relating to the $CO_2$ storage these numerical approaches are limited by computational constraints. To model the full problem is computationally expensive and difficult, if not impossible, to model the full problem at length and time scales appropriate for evaluating long-term storage security. This means that we need to structure the different scales in an appropriate manner. This is done in the model presented in Chapter 4.

**In Chapter 5** the numerical approach to solve the model derived in Chapter 4 is described. The numerical tools and the stabilization restrictions we need are given. We also discuss some of the problems and challenges we have had solving this model.

**In Chapter 6** we describe the problem the model in Chapter 4 is applied to. The parameters chosen are motivated by the Svalbard benchmark by Dahle et al. [9]. We present some of the numerical results from the model derived in Chapter 4.

**In Chapter 7** a summary is given together with conclusions we have drawn from this study.

# Chapter 1

# Geological storage of CO$_2$

*Geological storage of CO$_2$* corresponds to injecting and storing CO$_2$ in deep geological formations. In this chapter we give a general overview of geological storage and discuss the main challenges for its practical application. Furthermore, some of the challenges attached to this concept are discussed.

## 1.1 Background

Geological storage involves injection of captured CO$_2$ into deep geological formations. Of the different geological formations *deep saline aquifers* are the most ubiquitous and offers the largest potential storage volume [1]. In addition, deep saline aquifers can be used immediately in contrast to oil and gas reservoirs that must be exploited first. For these reasons, deep saline aquifers are very attractive for geological storage of CO$_2$. A deep saline aquifer consists of deep sedimentary rocks saturated with formation water or *brine*. The term brine is used for water saturated with or containing large amounts of a salt, especially of sodium chloride. According to U.S. Geologic Survey (USGS) classification, water classified as brine contains more than 35,000 ppm (parts per million) total dissolved solids of salt.

To increase the storage volume the CO$_2$ is injected at *super-critical state*, [15]. Having the CO$_2$ in super-critical state means that temperatures $T$ and pressures $P$ are above the critical point, that is $T_c = 31, 1°$ C and $P_c = 7, 38$ M Pa, see Figure 1.1. CO$_2$ at super-critical state has higher density than in gas phase and smaller *viscosity* than in fluid phase. Viscosity will be defined in the next chapter . Given typical geothermal gradients the conditions for having the CO$_2$ in super-critical state are found at depths around 800m below sea level [3].
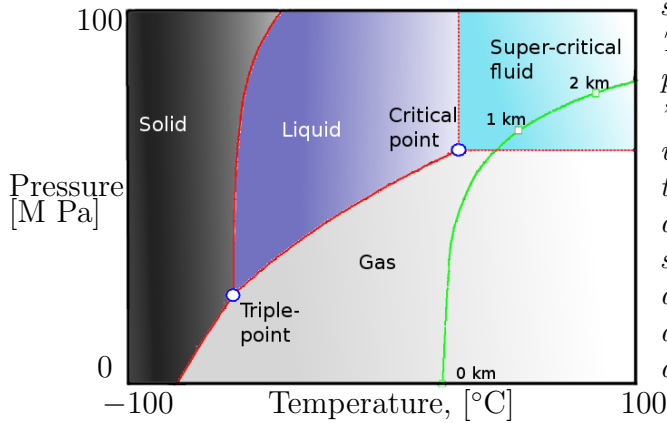
Figure 1.1:  *Illustration of the super-critical state for a phase.   The pressure is given in a logarithmic scale. The point between solid, liquid and gas phase is called the "triple-point".   The "critical-point" is also marked.   In green we see a phase diagram for CO$_2$ given a typical geothermal gradient of $30°C/km$ and surface temperature of $25°C$.   We see that CO$_2$ reaches super-critical state around $800m$ below sea level.   Data adapted from [33] and figure modified after [25].*

When CO$_2$ is in super-critical state it is only slightly soluble with water. Moreover, super-critical CO$_2$ have densities from 250-750kg/m$^3$ and viscosities between 2-20% of brine at typical pressure and temperature ranges of deep aquifers [24]. As indicated, if we look at injection of supercritical CO$_2$ in a deep saline aquifer we have that the supercritical CO$_2$ is less dense than the formation brine. As a consequence of this density difference the injected CO$_2$ spreads on top of the brine. We say that the CO$_2$ is more *buoyant* than the formation brine. Because of buoyancy forces CO$_2$ forms a gravity tongue as shown in Figure 1.2.
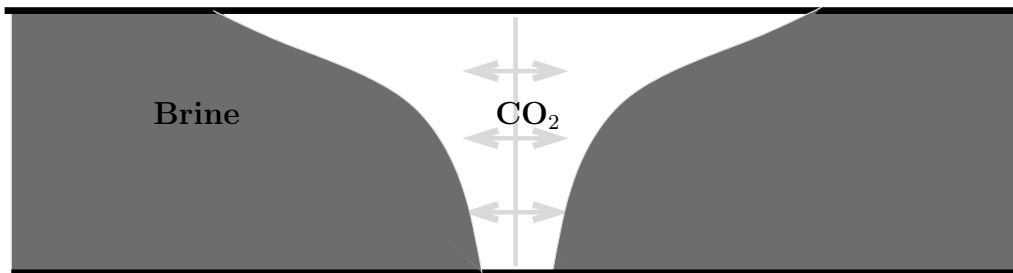


Figure 1.2: *The injected CO$_2$ phase will form a gravity tongue on top of the more dense formation brine.*

## 1.2    Trapping Mechanisms

Once the CO$_2$ is injected underground, different trapping mechanisms keep it securely stored and prevents the CO$_2$ from migrating back to the atmo-

sphere. It is common to divide these trapping mechanisms into four different categories:*1)structural and stratigraphic, 2)residual or capillary, 3)solubility or dissolution* and *4)mineral* trapping, [18, 19]. These four mechanisms will be described in the next paragraphs.

## Structural and Stratigraphic Trapping

When supercritical $CO_2$ is injected into a deep saline aquifer strong buoyancy forces act and the $CO_2$ plume migrates upwards until reaching the aquifer *cap rock*. A cap rock is an impermeable rock. Trapping by such a seal is called structural or stratigraphic trapping, or hydrodynamic trapping. This mechanism is very important and it actually is a prerequisite for any storage site because it prevents the rise of $CO_2$ during the time required for other trapping mechanisms to come into effect [5].

## Residual or Capillary Trapping

When supercritical $CO_2$ is injected into the formation it displaces brine as it moves through the aquifer. As $CO_2$ continues to move, brine occupies areas previously filled with $CO_2$. Some $CO_2$ will be left behind as disconnected or residual droplets surrounded by brine. This trapping mechanism is called residual trapping or capillary trapping. This process can be seen as a retention and immobilization of $CO_2$. Due to this we can imagine that a trail of residual $CO_2$ is left behind the mobile $CO_2$ as it moves through the aquifer.

## Solubility or Dissolution Trapping

Over time, $CO_2$ moves and large amounts of $CO_2$ will dissolve into the resident brine. Brine with dissolved $CO_2$ has higher density than pure brine and it migrates to deeper regions where more pure brine is available for further dissolution. This mechanism is called solubility or dissolution trapping.

## Mineral Trapping

When $CO_2$ is dissolved in brine, it can be immobilized for long time and geochemical binding to the rock can take place. That is, $CO_2$ can be trapped in minerals. This process is called mineral trapping, and will not be further discussed in this thesis.

## 1.3    Temporal and Spatial Scales

Each trapping mechanism contribution to the total trapping depends on a combination of several physical and geochemical processes that are active on different time scales. The spatial scale vary from the lateral extent of the plume migration of the order of hundred kilometers to the scale of different processes like dissolution, which occurs on a scale of $10^{-6}$m. When it comes to the temporal scale the different trapping mechanisms also occurs on different times. On a short time scale structural and stratigraphic trapping are the dominant trapping mechanism. The contribution of residual, solubility and mineral trapping increases over time. Also, with time the storage security increases [1]. The different trapping contributions is illustrated in Figure 1.3. adapted from [1] and modified by [14].
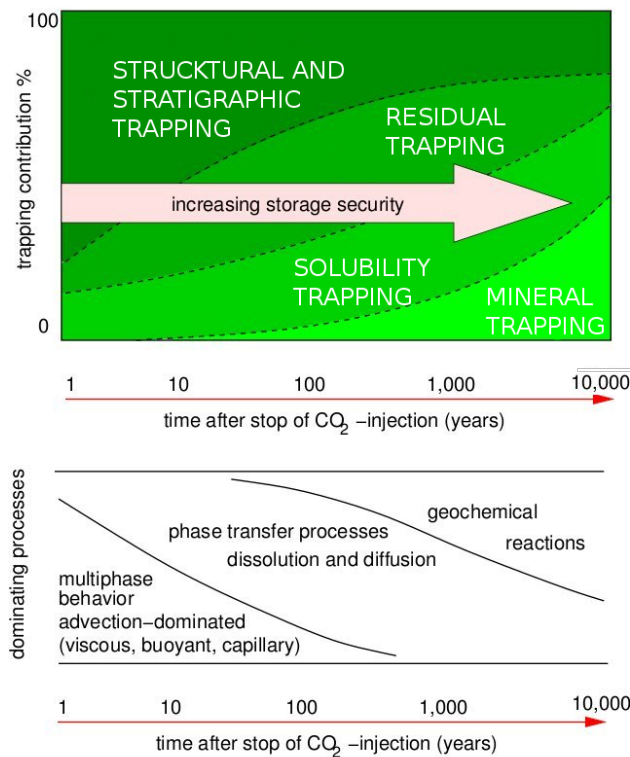
Figure 1.3: *Trapping contribution and storage security depending on different trapping mechanisms, and dominating processes over time, adapted from [1] and modified by [14].*

## 1.4   Challenges

Both the migration and trapping processes are inherently complex, spanning multiple spatial and temporal scales. The mathematical description of the complete system is very complex. This means that modeling the full problem at scales appropriate for evaluating long term storage is computationally expensive and difficult, if not impossible. This means that we need to structure the different scales in an appropriate manner.

# Chapter 2

# Theory from Reservoir and Fluid Mechanics

We introduce different concepts and definitions to understand and model the trapping mechanisms discussed in the previous chapter. Here, we give an introduction to different concepts and definitions and derive basic equations that are used in reservoir engineering and fluid mechanics. This will give us a framework for the further developments in later chapters.

## 2.1 Porous Media

Recall that deep saline aquifers are used for geological storage of $CO_2$. Such aquifers consists of sedimentary rocks. Between these solids there is a network of *pores* or void space. In Reservoir and Fluid Mechanics such a substance is referred to as a *porous media* [6]. The pores are a complex structure of connected and isolated pores, see Figure. 2.1. When modeling flow in porous
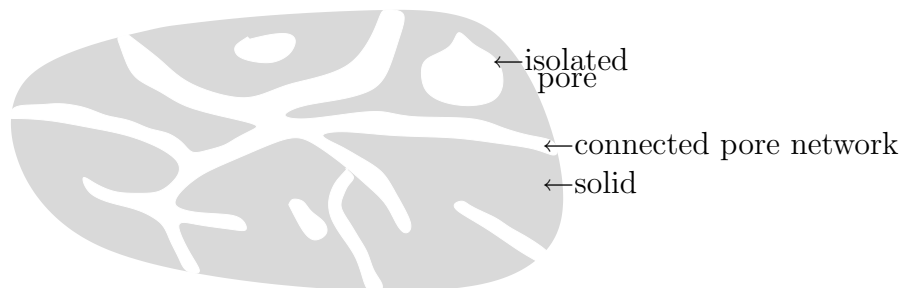


Figure 2.1: *A porous media with a connected pores, isolated pores and solid medium.*

media one must consider the irregularities of the pore network as random

variations with a well defined average. This means that quantities within a porous media are considered as averages over a *representative elementary volume* (REV) of the medium around the point considered [6].

Each fluid present in a porous media is called a *phase*. For example, brine in deep saline aquifers is considered as a phase. The phases can move with in the connected pores, and the governing equations for this movement will be presented throughout this chapter.

The connected (effective) pore volume, $V_Pp$, is the actual volume of the pores where the phases can move in. The ratio between the connected pore volume and the total volume, $V_T$, of the medium is called the *effective porosity $\phi$*, of the porous medium, i.e.

$$\phi \;=\; \frac{V_P}{V_T}.$$

Usually this dimensionless quantity is expressed as a percentage. From now on, we will refer to the effective porosity as the porosity. Note that the porosity is a property of the rock. In the next section some properties of the fluid or the phases will be presented.

## 2.2   Properties of a Fluid Phase

These properties concerns each individual phase regardless of how many phases that are present in the system.

Each fluid phase has a *density $\rho$*, which is mass of fluid per unit volume with units of $[\text{kg/m}^3]$ in the SI system. The *viscosity $\mu$* of a fluid phase reflects the internal resistance to flow of that phase. For example, water has low viscosity, while oil has high viscosity. Since this property reflects resistance the SI-unit is $[\text{Pa s}] = [\text{kg/ms}]$.

In fluid mechanics the *compressibility $c$* of a phase is a measure of the volume change of the phase due to a pressure change in the phase. The compressibility is defined as;

$$c \;=\; -\frac{1}{V}\frac{dV}{dp} = \frac{1}{\rho}\frac{d\rho}{dp},$$

where $V$ is total volume and $p$ is the pressure [29].

When more than one phase is present in the system the physics becomes

more complicated and we need to define additional quantities to describe the dynamics.

## 2.2.1 Miscible and Immiscible Displacement

When two or more phases are present in a porous media, two types of flow is possible; *miscible* and *immiscible* displacement. When two phases can dissolve in each other it is called miscible flow. Immiscible fluids are fluids that do not dissolve in one another.

For the $CO_2$ problem, the $CO_2$ is "slightly miscible" with the resident brine, meaning that relatively small (but significant) amounts of $CO_2$ can dissolve into the brine [25].

## 2.2.2 Saturation

When more than one phase is present we need a quantity that describes how much volume that is occupied by each phase compared to the effective volume of the pores. The *saturation $s_\alpha$* of a phase $\alpha$ describes exactly this relation and is defined as

$$s_\alpha \quad = \quad \frac{\text{volume of phase } \alpha}{\text{volume of all connected pores}}.$$

Since the pore-space always must be completely filled with fluids, we have that;

$$\sum_i s_i = 1.$$

The concept *residual saturation* reflects the minimum saturation that is attainable for a phase when displaced by another phase, this saturation is denoted $s_{\alpha r}$. We will describe this displacement later in this chapter and return to the residual saturation through this.

## 2.2.3 Wetting and Non-Wetting Fluid

With two phases present, one of the phases will be called *wetting* phase and the other the *non-wetting* phase. This is also the case when $CO_2$ and brine is present. The $CO_2$ phase is the non-wetting phase whilst brine is the wetting phase. In general a phase with small contact angle $(\theta < \frac{\pi}{2})$ with the rock is called a wetting phase. For a phase with contact angle $\theta > \frac{\pi}{2}$ the phase is called the non-wetting phase, see Figure 2.2.

Figure 2.2: *Wetting ($\theta < \pi/2$) and non-wetting phase ($\theta > \pi/2$).*

### 2.2.4  Several Components in a Phase

Sometimes we are not only interested in the overall fluid phase, but in one or more of the components that make up that phase. Components migrate from one phase to another through inter-phase mass transfer mechanisms. If we denote a component within the fluid phase by superscript $i$, the concentration of the component may be defined on a mass basis as the mass fraction $m_\alpha^i$;

$$m_\alpha^i = \frac{\text{mass of the component } i \text{ in phase } \alpha}{\text{total mass in phase } \alpha} = \frac{M_\alpha^i}{\sum_i M_\alpha^i}.$$

For notational purpose we mark that subscript always refers to phases and superscript to components, hence

$$m_\alpha^i \begin{array}{l} {}^{i} \longleftarrow \text{ component,} \\ {}_{\alpha} \longleftarrow \text{ phase.} \end{array}$$

Furthermore, we use superscript *mix* to indicate a mixture or *pure* to indicate a single component phase. For density that is

$$\rho_\alpha = \rho_\alpha^{mix} = \frac{\sum_i M_\alpha^i}{V_\alpha},$$

where $V_\alpha$ is the volume of phase $\alpha$. In regions with no mixing $\rho_\alpha = \rho_\alpha^{pure}$.

The mass fraction is a way of expressing concentration in a dimensionless form, multiplying the mass fraction with $\rho_\alpha^{mix}$

$$\rho_\alpha^{mix} m_\alpha^i = \frac{\sum_i M_\alpha^i}{V_\alpha} \frac{M_\alpha^i}{\sum_i M_\alpha^i} = \frac{M_\alpha^i}{V_\alpha} = \rho_\alpha^i.$$

For the $CO_2$ problem we noted that some of the $CO_2$ will dissolve into the brine since $CO_2$ is slightly miscible in brine. This $CO_2$ will be transported as a dissolved component with the brine. This leads to a component transport mechanisms that can be important on long time scales.

## 2.3   Darcy's Law

Darcy's law is an empirical relationship for water flow in a porous media first discovered through experiments by Henry Darcy in 1856. Later it has been shown that it is valid for any *Newtonian fluid*, see for example [11]. It establishes that the volumetric flow rate is a function of the flow area, elevation, fluid pressure and a proportionality constant. The law is stated in several different equivalent forms depending on the flow conditions. A general form of Darcy's Law for single phase flow is

$$\boldsymbol{u} \;=\; -\frac{\mathbf{k}}{\mu}\left(\nabla p + \rho\boldsymbol{g}\right), \tag{2.1}$$

where $\boldsymbol{u}$ is called the Darcy velocity or volumetric flux. This form of Darcy's Law is usually used in petroleum reservoir engineering. Here $\mathbf{k}$ is the *permeability* and $\mathbf{g}$ is the gravity vector. The permeability is the mentioned proportionality constant and this quantity tells us how easy the fluid will move through the porous medium.

When a property like permeability changes value depending on the direction being considered, the system referred to as *anisotropic*. When there are no directional differences the system is called *isotropic*. Furthermore, when a parameter changes as a function of spatial location the system is called *heterogeneous*. Conversely, when a system is spatially uniform it is called *homogeneous*. Mathematically this means that when a system is anisotropic and heterogeneous we denote the permeability with a second order tensor.

## 2.4   Multiphase Extension of Darcy's Law

When more than one phase is present in a system a new factor is introduced into Darcy's Law to reduce the apparent permeability. This factor accounts for the reduction in permeability as a result of the presence of the other phase. This is a function of $s_\alpha$ called the *relative permeability*, which is denoted $k_{r\alpha}(s_\alpha)$. If we introduce the mobility;

$$\lambda_\alpha = \frac{k_{r\alpha}}{\mu_\alpha},$$

we get Darcy's law for the phase $\alpha$:

$$\boldsymbol{u}_\alpha \;=\; -\mathbf{k}\lambda_\alpha\left(\nabla p_\alpha + \rho_\alpha\mathbf{g}\right). \tag{2.2}$$

The relative permeability is usually taken to be a nonlinear function of saturation. This function goes to zero before the actual phase saturation is zero. Recall, that this saturation value was called residual saturation. That is, some amount of the phase is present but fails to form a continuous pathway where flow flow can take place.

When dealing with flow in porous media a knowledge of the function among relative permeability and saturation is essential. For this purpose the *normalized water saturation* is defined as

$$s_{wn} = \frac{s_w - s_{wr}}{1 - s_{wr} - s_{nr}},$$

where subscript $w$ represents the wetting phase and subscript $n$ the non-wetting phase. In 1964 R.H. Brooks and A.T. Corey [8] proposed the following approximation to estimate the relative permeability curves of the two phases,

$$k_{rw} \approx s_{wn}^4, \tag{2.3}$$

$$k_{rn} \approx (1 - s_{wn})^2(1 - s_{wn}^2). \tag{2.4}$$

## 2.5 Capillary Pressure and Hysteresis Phenomena

In general, a pressure difference exists across the interface separating two fluid phases. The magnitude of this pressure difference depends on the curvature of this interface [6], see Figure 2.3. The difference in the phase pressures
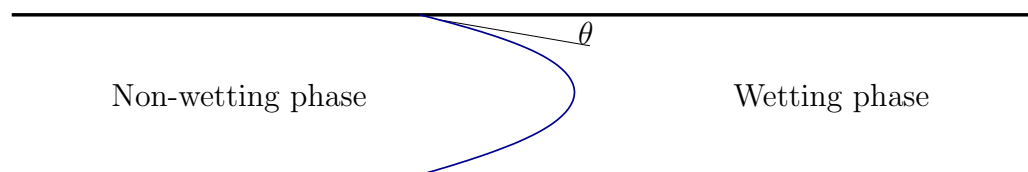


Figure 2.3: *Non-wetting and wetting fluid phase in a pipe with an interface separating them.*

between the non-wetting and the wetting phase is called *capillary pressure* $P_c$, i.e.

$$P_c = p_n - p_w,$$

where subscript $n$ and $w$ indicates the phase pressure of the non-wetting and wetting phase respectively. The value of $P_c$ depends on saturation and on

the geometry in which the interface occurs, being larger in small spaces than in large spaces for a given saturation [8].

When one phase is displaced by another, we distinguish between *imbibition* and *drainage*. *Imbibition* is defined as the displacement of a non-wetting by a wetting phase. *Drainage* is displacement of a wetting phase by a non-wetting phase. The phase that initially saturates an area is displaced by the other phase. In this displacement the contact-angle between the phases depends on whether equilibrium is reached during a drainage or an imbibition process. Consequently the capillary pressure depends on the flow itself and this phenomenon is called the *hysteresis effect*. The hysteresis effect is illustrated in Figure 2.4. Note that the two processes are not reversible in the sense that
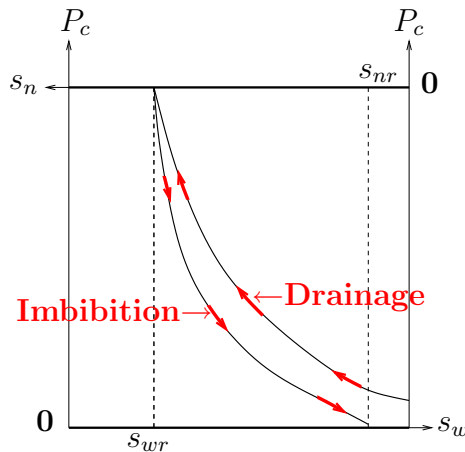


Figure 2.4: *The capillary pressure depending on whether there is an imbibition or a drainage process.*

an imbibition process do not follow a drainage curve in the opposite direction. No matter how much the capillary pressure is increased in an drainage process the saturation for the wetting phase will not go below the value $s_{wr}$. Similarly, the saturation of the non-wetting phase in an imbibition process does not go below a certain level $s_{nr}$. These values are what we call the residual saturation or the minimum attainable saturation [20].

This can be illustrated by the knowledge the wetting phase has a higher tendency to agglutinate to the rock than to the non-wetting phase. As a result of this a thin film of the wetting fluid around the rock will be left behind during the drainage process. Similarly, during an imbibition process regions of disconnected non-wetting fluid phase will be left behind as it is imbibed by a wetting phase. This is illustrated in Figure 2.5:

wetting phase

non-wetting phase

wetting phase

non-wetting phase

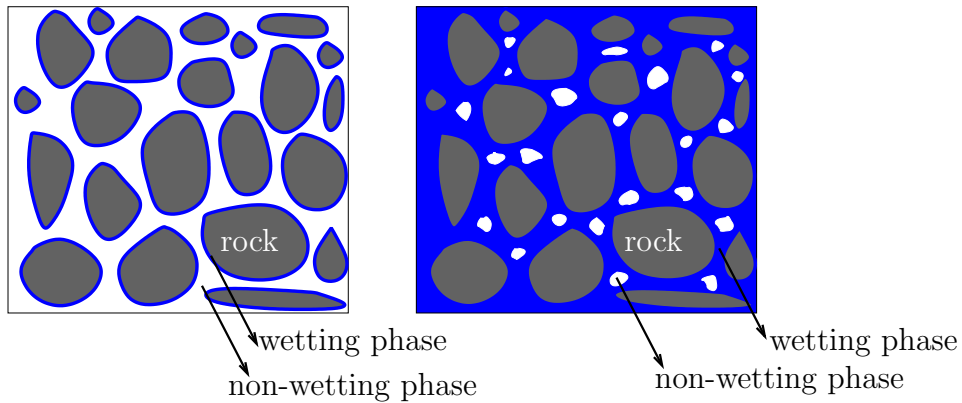Figure 2.5: *Wetting phase left behind in a drainage process to the left, and non-wetting phase left behind in an imbibition process to the right. The wetting phase is blue and the non-wetting phase is white.*

## 2.6 Governing Equations

In this section we present equations that describes single and two-phase flow in porous media at the fine scale. In this section we introduce a conservation equation for the mas of each fluid phase. By certain modeling choices or simplifications, we gain two important modeling equations, one for saturation and one for the pressure. Finally, we introduce an equation for the random molecular motion within a fluid which corresponds to a diffusion equation.

### 2.6.1 Mass Conservation Equation

Conservation laws tells us how an *extensive* physical quantity $\varphi$ is conserved within a closed system. An extensive property of a system depends on the system size or the amount of material in the system. Such quantities are for example mass and volume. By contrast an *intensive* property does not depend on the system, such as density, pressure, viscosity, etc. To derive such conservation equations we must account for processes that influence the extensive property.

We look at a fixed reference volume $\Omega$, see Figure 2.6, with boundary $\partial\Omega$ and outward normal $\mathbf{n}$. Fluid may leave or enter the volume through source or sink term $Q$, e.g. a well. We do a balance between the quantities entering/leaving the volume through the edge $\partial\Omega$ or possible sources or sinks $Q$ and the rate of change of the total mass inside $\Omega$

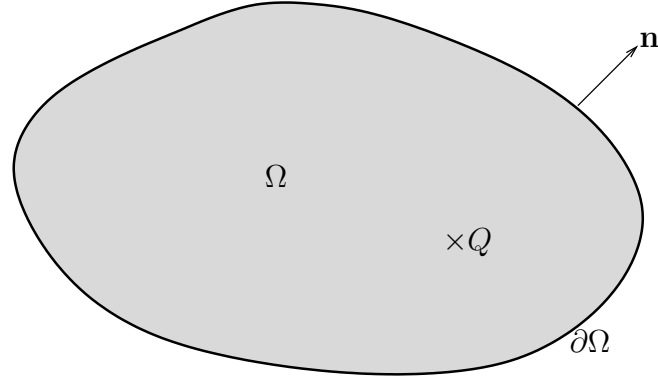$$\{\text{Accumulation}\} + \{\text{Net Rate of Out flux}\} = \{\text{Sources/Sinks}\},$$

Figure 2.6: *Fixed reference volume $\Omega$, with boundary $\partial\Omega$ and source $Q$. The outward normal is denoted* **n**.

where the unit is the unit of $\varphi$ per unit time. A mathematical expression for this is

$$\frac{d}{dt}\int_\Omega \varphi d\Omega + \int_{\partial\Omega} \boldsymbol{n} \cdot \boldsymbol{F} dS = \int_\Omega q d\Omega, \qquad (2.5)$$

where **n** is the outward normal, **F** is the flux and $q$ represents the sources and sinks. For the quantity being mass, this is

$$\varphi = \rho\phi$$
$$\mathbf{F} = \rho\mathbf{u},$$

where **u** is the Darcy velocity, $\rho$ the density and $\phi$ the porosity. The surface integral in equation 2.5) can be replaced by a volume integral using Gauss's Theorem. Further, we can use *Leibniz integral rule*;

$$\frac{d}{dt}\int_\Omega f(x,t) \ d\Omega = \int_\Omega \frac{\partial f}{\partial t} \ d\Omega,$$

to move the $d/dt$ inside the integral. We can do this since $\Omega$ is not time dependent. Since the volume is arbitrary and the integrand continuous we get the differential form of the Mass Conservation Equation for single phase flow

$$\frac{\partial(\rho\phi)}{\partial t} + \nabla \cdot \rho\mathbf{u} = q. \qquad (2.6)$$

For multi-phase-flow the saturation also comes into account, and the Mass Conservation Equation (2.6) for phase $\alpha$ is

$$\frac{\partial(\rho_\alpha s_\alpha \phi)}{\partial t} + \nabla \cdot \rho_\alpha \mathbf{u}_\alpha = q_\alpha. \qquad (2.7)$$

## 2.6.2   Saturation and Pressure Equation

It is sometimes useful and necessary to make some simplifications and assumptions that are physically justified. In what follows we will consider that:

- fluids are incompressible, $c = 0$ ($\rho$=constant),

- phases are immiscible and have constant viscosity $\mu$,

- two-phase fluid system, with a wetting ($w$) and a non-wetting ($n$) phase,

- constant porosity $\phi$.

We introduce the *total velocity*;

$$\boldsymbol{u} = \boldsymbol{u}_n + \boldsymbol{u}_w.$$

By adding equation (2.7) for both the wetting and the non-wetting phase we have that

$$\nabla \cdot \boldsymbol{u} \;\; = \;\; \frac{q_w}{\rho_w} + \frac{q_n}{\rho_n} \equiv q, \tag{2.8}$$

since $\partial/\partial t(s_n + s_w) = \partial/\partial t(1) = 0$. Multiplying Darcy's Law (2.2) for both the wetting and the non-wetting phase, with the mobility for the opposite phase we get the expressions:

$$\lambda_n \boldsymbol{u}_w \;\; = \;\; -\mathbf{k}\lambda_n\lambda_w \left( \nabla p_w + \rho_w \boldsymbol{g} \right),$$

$$\lambda_w \boldsymbol{u}_n \;\; = \;\; -\mathbf{k}\lambda_w\lambda_n \left( \nabla p_n + \rho_n \boldsymbol{g} \right).$$

Subtracting these and using the expression for the total velocity we get the expression:

$$\boldsymbol{u}_w \;\; = \;\; \frac{\lambda_w}{\lambda_w + \lambda_n}\boldsymbol{u} + \boldsymbol{k}\frac{\lambda_n\lambda_w}{\lambda_w + \lambda_n} \left( \nabla P_c + (\rho_n - \rho_w)\boldsymbol{g} \right). \tag{2.9}$$

We now define $s = s_w$ and

$$f(s) \;\; \equiv \;\; \frac{\lambda_w}{\lambda_w + \lambda_n}.$$

Then we substitute our expression (2.9) into the Mass Conservation Equation (2.7) for the wetting phase;

$$\phi\frac{\partial s}{\partial t} + \nabla \cdot f(s) \left( \boldsymbol{u} + \boldsymbol{k}\lambda_n(\nabla P_c + (\rho_n - \rho_w)\boldsymbol{g}) \right) \;\; = \;\; \frac{q_w}{\rho_w}, \tag{2.10}$$

this is the *Saturation Equation.*

The total velocity by adding Darcy's Law (2.2) for both phases is

$$\boldsymbol{u} = \boldsymbol{u}_w + \boldsymbol{u}_n = -\boldsymbol{K}\left(\lambda_w(\nabla p_w + \rho_w \boldsymbol{g}) + \lambda_n(\nabla p_n + \rho_n \boldsymbol{g})\right).$$

Taking the divergence on both sides and using the expression (2.8), we have that:

$$\nabla \cdot \boldsymbol{u} = -\nabla \cdot \boldsymbol{k}\left(\lambda_w(\nabla p_w + \rho_w \boldsymbol{g}) + \lambda_n(\nabla p_n + \rho_n \boldsymbol{g})\right) = q, \qquad (2.11)$$

which gives an equation for the pressure.

### 2.6.3   Diffusion Equation

Movement of molecules within a fluid is called *convection.* It is a heat transfer mode that is comprised of two mechanisms. One is energy transfer due to random molecular motion, this is called *diffusion.* Energy is also transfered by the bulk motion of the fluid, which is called *advection* [17]. These two mechanisms generates different flux terms

$$\begin{aligned} \boldsymbol{F}_D &= \boldsymbol{J} &\text{for diffusion,} \\ \boldsymbol{F}_A &= \rho m_\alpha^i \boldsymbol{u} &\text{for advection.} \end{aligned} \qquad (2.12)$$

The diffusive flux $\boldsymbol{J}$ and will be defined below and $m_\alpha^i$ is the mass fraction. This flux term also includes what is called mechanical mixing or mechanical dispersion. This mixing arises due to the velocity variability on a scale below the one used to define the average velocity [6].

The heat equation also known as the *Diffusion Equation* describes in typical applications the evolution in time of the density of some quantity $u$ such as heat, concentration, etc. In 1855 Adolf Fick postulated that for $u$ being the chemical concentration of a substance, the diffusive flux $\boldsymbol{J}$ is proportional to the concentration gradient at constant temperature [32]. Here the proportional constant is called the *diffusion coefficient $D$.* Since the diffusion is from regions of higher to lower concentration the flux density points in the opposite direction to the concentration gradient. This is

$$\mathbf{J} = -D\nabla C, \qquad (2.13)$$

where $C = C(\boldsymbol{x}, t)$ is the concentration and $\nabla$ is the gradient in terms of spatial derivatives. The concentration is dependent of the position $\mathbf{x}$ and the time $t$. Equation (2.13) is called *Fick's first law of Diffusion.*

From the Conservation Equation (2.5) with $q = 0$ we know that the rate of change of the total quantity within a volume equals the negative of the net flux through the boundary. If the quantity is taken to be the concentration $C$

$$\frac{\partial C}{\partial t} = -\nabla \cdot \boldsymbol{F}, \tag{2.14}$$

where $\mathbf{F}$ is the flux density. If the diffusive flux $\mathbf{F}_D = \mathbf{J}$ is inserted in equation (2.14) and the diffusion coefficient is taken to be constant, this is

$$\frac{\partial C}{\partial t} - D\nabla^2 C = 0, \tag{2.15}$$

that is the Diffusion Equation. This equation yields an equation for the non-advective motion in a fluid and is also called *Fick's second law of diffusion*. This equation can be solved analytically and the solution is of importance when looking at diffusion problems such as dissolution of $CO_2$ into brine.

In one dimension the Diffusion Equation (2.15) is

$$\frac{\partial C}{\partial t} - D\frac{\partial^2 C}{\partial x^2} = 0.$$

with initial and boundary conditions

$$C(x,0) = 0, \qquad C(0,t) = C_0.$$

The analytical solution of this PDE is

$$C(x,t) = C_0 \text{erfc}\left(\frac{x}{2\sqrt{Dt}}\right), \tag{2.16}$$

where $\text{erfc}\,(\;\cdot\;)$ is the *complementary error function*. The length $2\sqrt{Dt}$ is called the *diffusion length*. The *error function* is defined as

$$\text{erf}\,(x) = \frac{2}{\sqrt{\pi}} \int_x^\infty e^{-t^2} \text{dt},$$

and the complementary error function is $\text{erfc}(x) = 1 - \text{erf}(x)$. An approximation to the error function can be found by utilizing the first term in its Taylor Series. This gives an approximate solution to the diffusion equation in one dimension

$$C(x,t) \approx C_0\left(1 - \frac{x}{\sqrt{Dt\pi}}\right). \tag{2.17}$$

## 2.7 Fine and Coarse scale

The governing equations presented in the previous sections represents the full three-dimensional flow. This representation can be interpreted as a fine scale representation and we note that we have used small letters for the parameters introduced so far. When considering flow in porous media in subsurface formations it is convenient to take advantage of the fact that the horizontal extent is much larger than the vertical extent. Since the movement in the vertical direction is bounded by the top and bottom of the aquifer which gives a very limited region to flow in compared to the horizontal extent. This again motivates to neglect the vertical velocity. If the fine scale equations are integrated over the vertical dimension the equations are reduced to two-dimensional equations. This two-dimensional representation is what we interpret as the coarse scale representation. This concept will be illustrated and used in the next two chapters.

# Chapter 3

# Model for Residual Trapping

In this chapter we develop a physical and mathematical model for *residual trapping* introduced in Chapter 1. The model introduced here is similar to other works , e.g. [13, 16, 18, 24]. We note that the effect of dissolution is not included in the model derived in this chapter . This is an assumption that warrants further discussion and study, and we will return to this in Chapter 4.

## 3.1 Background

Recall from Chapter 1 that when $CO_2$ is injected in a deep saline aquifer the formation is initially saturated with brine. In addition we consider an aquifer that has a dip angle $\theta > 0$. From now on the non-wetting $CO_2$ phase is denoted with subscript $c$ and brine with $b$. In a deep (below 800m) and "cold" (surface temperature of $T = 10°C$ and geothermal gradient of $25°C/km$) geological formation the phase properties are found [25] to be:

| Phase | Density | Viscosity |
|-------|---------|-----------|
| Brine | 995-1202 kg/m$^3$ | $0.378 \cdot 10^{-3} - 0.644 \cdot 10^{-3}$ kg/m s |
| $CO_2$ | 733 kg/m$^3$ | $0.0611 \cdot 10^{-3}$ kg/m s |

We see that $CO_2$ is much less viscous and less dense than brine $\rho_c < \rho_b$. Hence, the injected $CO_2$ spreads on top of the brine. For simplification we take the thickness of the aquifer to be constant and equal to $H$. We take the $z$-axis to be perpendicular to the formation and oriented upwards. The $(x, y)$ coordinates are taken to be in the aquifer plane and parallel to the formation flow or the lateral extent as shown in Figure 3.1. Figure 3.1 shows the movement in the $(x, z)$ plane. An interface between the injected $CO_2$
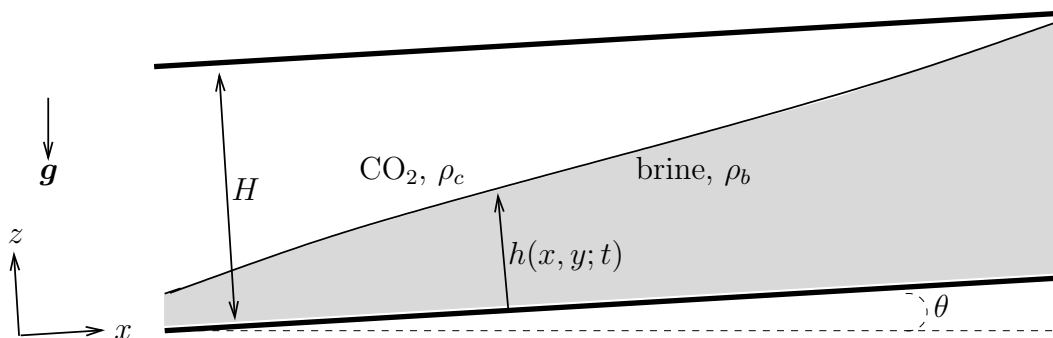
25

Figure 3.1: *An illustration of the aquifer with the $CO_2$ (white) spreading on top of the brine(gray). A interface $z = h(x, y; t)$ between the two phases is also drawn.*

and brine is drawn and the thickness of the position of the interface between both fluids is taken to be $z = h(x, t)$. The unit vectors are denoted $e_1$ in the $x$-direction, $e_2$ in the $y$-direction and $e_3$ in the $z$-direction, such that the gravity vector is

$$\boldsymbol{g} \quad = \quad -g \sin \theta \boldsymbol{e}_1 - g \cos \theta \boldsymbol{e}_3.$$

Injected $CO_2$ displaces brine in a drainage process. As explained in Chapter 2 some residual brine will be left behind. At the same time, brine imbibes into the mobile $CO_2$ in the back end of the $CO_2$ plume and a trail of residual $CO_2$ is left behind as the $CO_2$ plume migrates. This trail or this region of immobile $CO_2$ is referred to as the residually trapped $CO_2$.

## 3.2   Approximations

In order to come up with relatively simple equations that can model the $CO_2$ migration over time, the complexity of the system must be reduced. In this section three approximations will be described and argued for.

### 3.2.1   Sharp Interface

As mentioned the density difference between the two phases implies strong buoyancy forces in our system. This allow for the system to be simplified by assuming that the heaviest phase settles near the bottom and the lightest phase rises to the top of the formation. This is called *gravity segregation.* In reality there will always be a transition zone between the $CO_2$ and brine phase, so called *capillary fringe* [26]. This transition zone is often neglected and the system is simplified by assuming a *sharp interface* between the two

phases. By assuming a sharp interface the medium is assumed to either be filled with brine or with $CO_2$. This means that the saturations above and below the interface are assumed constant.

For the saturation for the non-wetting phase we know that the formation is initially saturated with brine, then $s_c = 0$ everywhere. When $CO_2$ is injected it drains the brine and the saturation is then $s_c = 1 - s_{wr}$. As the $CO_2$ plume starts to migrate brine imbibes into parts of the $CO_2$ region. Below the $CO_2$ in residual saturation and the mobile $CO_2$ pure brine is still present. This results in the saturation distribution

$$s_c = \begin{cases} 0, & \text{if } 0 \leq z < h_{min}(x, y; t) \\ s_{cr}, & \text{if } h_{min}(x, y; t) \leq z < h(x, y; t) \\ 1 - s_{br}, & \text{if } h(x, y; t) < z \leq H, \end{cases}$$

where $z = h(x, y; t)$ is the unknown location of the interface between residual and mobile $CO_2$ at the time $t$. The variable $h_{min}(x, y; t')$ represents the interface between the residual $CO_2$ and the pure brine,

$$\begin{aligned} h_{min}(x, y; t') &= \min_{t \in [0, t']} h(x, y; t), \\ h_{min} &\leq h. \end{aligned}$$

### 3.2.2   Vertical Equilibrium

For typical geological formations where $CO_2$ is injected the vertical extent is on the order of tens of meters. The horizontal extent where the plume spreads is on the order of several kilometers. This large aspect ratio ($L/H >> 1$) motivates us to neglect the flow in the vertical direction. Our formation is tilted and it is natural to think of negligible flow perpendicular to the formation in the $\boldsymbol{e}_3$ direction. This is the same as saying that both fluids are in vertical equilibrium.

If we assume that the aquifer is homogeneous and that the phase densities and viscosities are assumed constant between each of the interfaces, Darcy's law (2.2) with negligible flow in the direction perpendicular to the formation is

$$\boldsymbol{u}_\alpha \cdot \boldsymbol{e}_3 = -k\lambda_\alpha \left(\nabla p_\alpha - \rho_\alpha \boldsymbol{g}\right) \cdot \boldsymbol{e}_3 = 0. \tag{3.1}$$

Integrating this equation from a datum $d$,

$$\int\limits_{d}^{z} \left( \frac{\partial p_\alpha}{\partial z'} - \rho_\alpha \boldsymbol{g} \cdot \boldsymbol{e}_3 \right) \mathrm{d}z' \;\; = \;\; 0,$$

$$p_\alpha(x, y; z) - p_\alpha(x, y; d) \;\; = \;\; \boldsymbol{g} \cdot \boldsymbol{e}_3 \int\limits_{d}^{z} \rho_\alpha \mathrm{d}z'. \tag{3.2}$$

This is an expression for hydrostatic equilibrium, where $p_\alpha(x, y; d)$ is some datum pressure.

We neglect the capillary pressure along the interface between the phases, meaning that the phase pressures are equal along this interface. We have that knowledge of the pressure at one point in the $\boldsymbol{e}_3$ direction and of the location of the interface $h$ - allows us to calculate the pressure at all other locations in the $\boldsymbol{e}_3$ direction.

### 3.2.3   Time Scales

As we discussed in Chapter 1 the different time scales associated with the different trapping mechanisms are believed to be quite different;

$$t_{\text{structural}} \quad \sim \quad t_{\text{residual}} \quad << \quad t_{\text{dissolution}} \quad << \quad t_{\text{mineral}}.$$

Thus it is justified to neglect dissolution and mineral trapping when studying $CO_2$ migration in an early period. In the model developed in the next chapter we no longer neglect dissolution.

## 3.3   Mathematical Model

Under the approximations discussed in the previous section we can take the vertical average of the Mass Conservation Equation (2.7) from Chapter 2;

$$\frac{\phi}{H} \int\limits_{0}^{H} \frac{\partial s_\alpha}{\partial t} \mathrm{d}z + \nabla \cdot \frac{1}{H} \int\limits_{0}^{H} \boldsymbol{u}_\alpha \mathrm{d}z \;\; = \;\; \frac{1}{H} \int\limits_{0}^{H} q_\alpha \mathrm{d}z. \tag{3.3}$$

Since we neglect flow in the $\boldsymbol{e}_3$ direction, the Darcy velocity $\boldsymbol{u}_\alpha$ only has components in the $(\boldsymbol{e}_1, \boldsymbol{e}_2)$ directions

$$\boldsymbol{u} \;\; = \;\; -k\lambda_\alpha \left( \nabla_{\parallel} p_\alpha + \rho_\alpha \boldsymbol{g}_{\parallel} \right). \tag{3.4}$$

Here the subscript $||$ is used to indicate that the vertical components are neglected, and

$$\begin{aligned}
\nabla_{||} &= \frac{\partial}{\partial x}\boldsymbol{e}_1 + \frac{\partial}{\partial y}\boldsymbol{e}_2, \\
\boldsymbol{g}_{||} &= -g\sin\theta\boldsymbol{e}_1.
\end{aligned}$$

From the vertical equilibrium assumption we know that the pressure distribution is hydrostatic (3.2). For the brine phase this is

$$p_b(x,y;z) = p_b(x,y;0) - g\rho_b\cos\theta z, \tag{3.5}$$

where $p_b(x,y;0)$ is the datum pressure at $z = 0$. In the previous section we neglected the capillary pressure along the interface $h(x,y;t)$, meaning that the pressures in the two phases are equal along the interface: $p_c(x,y;h) = p_b(x,y;h)$. Consequently the equation for for the $CO_2$-phase is;

$$p_c(x,y;z) = p_b(x,y;0) - g\cos\theta\left(\rho_b h + \rho_n(z-h)\right). \tag{3.6}$$

To obtain an equation for the evolution of the interface $h = h(x,y;t)$ we now follow the derivation of other works [16, 24, 13]. With the assumption of incompressible fluids and in the absence of source terms we recall from Chapter 2 that

$$\nabla \cdot \boldsymbol{u} = 0,$$

where $\boldsymbol{u} = \boldsymbol{u}_c + \boldsymbol{u}_b$ is the total velocity. If we now integrate this equation vertically over the aquifer;

$$\begin{aligned}
\int_0^H u_c\mathrm{d}z + \int_0^H u_b\mathrm{d}z &= 0, \\
u_b\,h + u_c\,(H-h) &= 0, \tag{3.7}
\end{aligned}$$

where the Darcy velocities $u_\alpha$ are the phase velocities in the $x$-direction. We insert the two different phase pressures in the Darcy velocities in the $x$-direction,

$$u_b = -k\lambda_b\left(\frac{\partial p_d}{\partial x} - g\rho_b\sin\theta\right), \tag{3.8}$$

$$u_c = -k\lambda_c\left(\frac{\partial p_d}{\partial x} - g(\rho_b - \rho_n)\cos\theta\frac{\partial h}{\partial x} - g\rho_n\sin\theta\right). \tag{3.9}$$

From this we obtain an equation for the unknown datum pressure $p_d$:

$$\frac{\partial p_d}{\partial x} = \frac{g(\rho_b - \rho_n)\left(\lambda_c(H-h)\frac{\partial h}{\partial x}\cos\theta + \lambda_b h\sin\theta\right)}{\lambda_c(H-h) + \lambda_b h} + g\rho_n\sin\theta. \tag{3.10}$$

We obtain the different coarse scale variables by integrating over the aquifer in the $\boldsymbol{e}_3$ direction:

$$S_c = \frac{1}{H}\int_0^H s_c \mathrm{d}z = \frac{1}{H}\left((h - h_{min})s_{nr} + (H - h)(1 - s_{wr})\right),$$

$$\Lambda_c(S_c) = \frac{1}{H}\int_0^H \frac{k_{rc}(s_c)}{\mu_c}\mathrm{d}z = \frac{1}{H}\left(\frac{k_{rc}(1-s_{br})}{\mu_c}(H - h_{min})\right), \qquad (3.11)$$

$$\Lambda_b(S_c) = \frac{1}{H}\int_0^H \frac{k_{rb}(s_c)}{\mu_b}\mathrm{d}z = \frac{1}{H}\left(\frac{k_{rb}(0)}{\mu_b}h_{min} + \frac{k_{wb}(s_{cr})}{\mu_b}(h - h_{min})\right).$$

We recall the constraint that $h_{min} \leq h$ and try to include the hysteresis effect on this problem. In other works like [13, 18] they have looked at the sign-change of $\partial h/\partial t$ to part between imbibition and drainage. This can be looked at as a simplified hysteresis model. In [26] Nordbotten and Dahle point out that if $h$ is growing with time ($CO_2$ drains the brine), then $h_{min} < h$. Furthermore, if $h_{min} \neq h$ then $h_{min}$ does not change with time. If we consider the change in $CO_2$ saturation with time this is,

$$\frac{\partial S_c}{\partial t} = \begin{cases} \dfrac{-(1 - s_{br})}{H}\dfrac{\partial h}{\partial t} & \text{if } h = h_{min}, \\ \dfrac{-(1 - s_{br} - s_{cr})}{H}\dfrac{\partial h}{\partial t} & \text{if } h \neq h_{min}. \end{cases}$$

If we consider flow in the $x$-direction and insert the coarse scale variables (3.11) in the absence of source terms in the Saturation Equation (2.10) we obtain the equation:

$$\frac{\partial h}{\partial t} + \kappa\frac{\partial}{\partial x}\left[\frac{(H - h)(h + \delta\lambda_b(h - h_{min}))}{(M - 1)h - MH + \delta\lambda_b(h - h_{min})}\left(\sin\theta + \cos\theta\frac{\partial h}{\partial x}\right)\right] = 0, \qquad (3.12)$$

where

$$\kappa = \begin{cases} \dfrac{\lambda_c\Delta\rho g k}{\phi(1 - s_{wr})} & h = h_{min}, \\ \dfrac{\lambda_c\Delta\rho g k}{\phi(1 - s_{wr} - s_{nr})} & h \neq h_{min}, \end{cases} \qquad M = \frac{\lambda_n(1 - s_{br})}{\lambda_b(0)} \quad \text{and} \quad \delta\lambda_b = \frac{\lambda_b(0) - \lambda_b(s_{rn})}{\lambda_b(0)}.$$

This model is similar to the model used in [13] and [18] except for the term $\delta\lambda_b$. These authors neglect this term and as discussed in [26] this is questionable.

## Discussion

Equation (3.12) is called a *non-linear advection diffusion* equation. That is an equation of the form

$$u_t + \underbrace{f(u)_x}_{advection} + \underbrace{(d(u)u_x)_x}_{diffusion} = 0,$$

and is a parabolic equation. In this model the diffusion-term is not due to physical diffusion, but due to the buoyancy forces in the system. In both [13] and [18] they make this equation dimensionless and neglects the diffusion-term in order to solve the equation analytically. For the $CO_2$ problem we have mentioned that the lateral extent $L$ typically is of several orders larger than the vertical height $H$. When the equation for the interface $h$ (3.12) is made dimensionless the coefficient $L/H$ appears in front of the diffusion term, and for $L >> H$ the diffusion term can be neglected. The resulting equation is a hyperbolic equation of the form

$$\frac{\partial \eta}{\partial \tau} + \sigma \frac{\partial}{\partial \xi} f(\eta) = 0. \tag{3.13}$$

Hesse et al. [13] consider this equation with the dimensionless initial condition

$$\eta(\xi, 0) = \begin{cases} \xi_L, & \xi < 0, \\ \xi_R, & \xi > 0. \end{cases} \tag{3.14}$$

This initial condition can represent a *finite release* of the mobile $CO_2$ considering a rectangular plume of $CO_2$. A problem of the form (3.13) with piecewise constant initial data having a single discontinuity like (3.14) is called a *Riemann problem*. The Riemann Problem is very useful for the understanding of hyperbolic partial differential equations like (3.13). We will not go into detail on the Riemann problem here, and neither solve the model problem given here analytically. Details can be found elsewhere, e.g. [21, 13].

# Chapter 4

# Modeling Dissolution Trapping

In Chapter 3 a framework for modeling residual trapping was introduced. As mentioned in Chapter 1 solubility trapping is the dominating trapping process on long temporal scales. This motivates us to use a model that includes this process when looking at the evolution of a $CO_2$ plume. In this chapter we develop an upscaled mass transfer model within the vertically averaged framework that includes dissolution trapping.

## 4.1   Dissolution of $CO_2$ into Brine

Recall from the previous chapter that the free phase $CO_2$ is separated from underlying brine by a relatively sharp interface. Across this interface $CO_2$
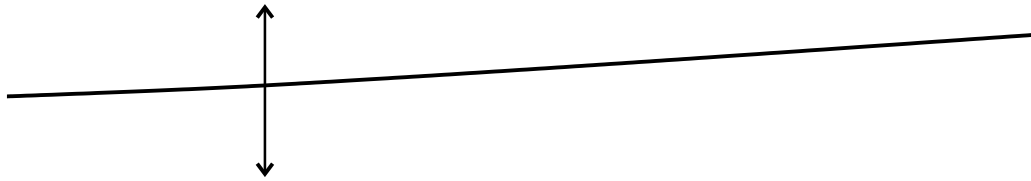
dissolves into pure brine (or opposite) and form a diffusive boundary-layer that grows with time. This type of dissolution can be interpreted as pure diffusion.

Most gases when dissolved in brine at reservoir conditions reduce the density of brine. However, $CO_2$ is one of the few gases that lead to a density increase [10]. The second type of dissolution comes from this density increase. Brine saturated with $CO_2$ can actually be up to 1% more dense than unsaturated brine. After some onset time this creates a gravitationally unstable configuration of denser brine saturated with $CO_2$ above less dense pure brine. When

this instability occurs, fingers with $CO_2$ saturated brine starts to propagate downwards, as illustrated in Figure 4.1(a). This mixing of $CO_2$ and brine is called *convective mixing*. In Figure 4.1(b) we see an example of a high
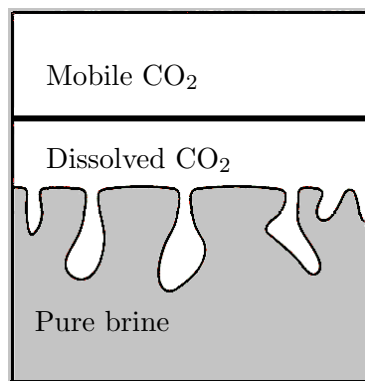


(a)
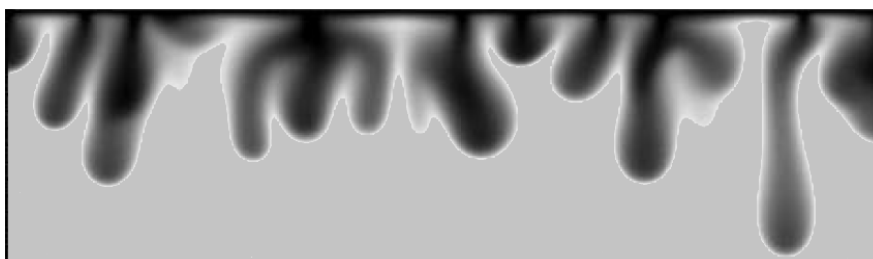


(b)

Figure 4.1: *Illustration of the fingering mechanism adapted and modified from [31]. In (a) we see the different regions with mobile and dissolved $CO_2$ above pure brine. In (b) we see a numerical simulation of dissolution by Riaz et al. [31], where the fingers are clearly visible.*

resolution numerical simulation of the dissolution process. We see the fingers with dissolved $CO_2$ migrating downwards.

We understand that we have two types if dissolution that must be distinguished,

- direct dissolution through the interface, pure diffusion,

- enhanced dissolution due to the convective mixing.

The effect of direct dissolution can be modeled in the framework developed in Chapter 3, but the effect is likely to be small compared to the residual

trapping [13]. In the long term the dominant mechanism for dissolution of $CO_2$ into brine is convective mixing. This enhanced dissolution is of several orders more important than pure diffusion [10]. To emphasize this we look at the dissolution rate for pure diffusion. Recall the one dimensional Diffusion Equation (2.15) with the analytical solution

$$C(x,t) \approx C_0 \left( 1 - \frac{x}{\sqrt{Dt\pi}} \right),$$

where $C$ now is the concentration of dissolved $CO_2$, and $D$ is the diffusion coefficient. If we look at the mass production rate of dissolved $CO_2$ per time, $C_R$;

$$C_R = \frac{\partial}{\partial t} \left( \frac{1}{\Delta L} \int_{x_1}^{x_2} C(x,t) \mathrm{d}x \right),$$

where $\Delta L$ is the length of the interface the $CO_2$ is dissolving through between $x_1$ and $x_2$. The dissolution rate for pure dissolution is shown in Figure 4.2 together with the dissolution rate due to convective mixing found numerically by Pau et al. in [28]. The convective mixing seems to accelerate the
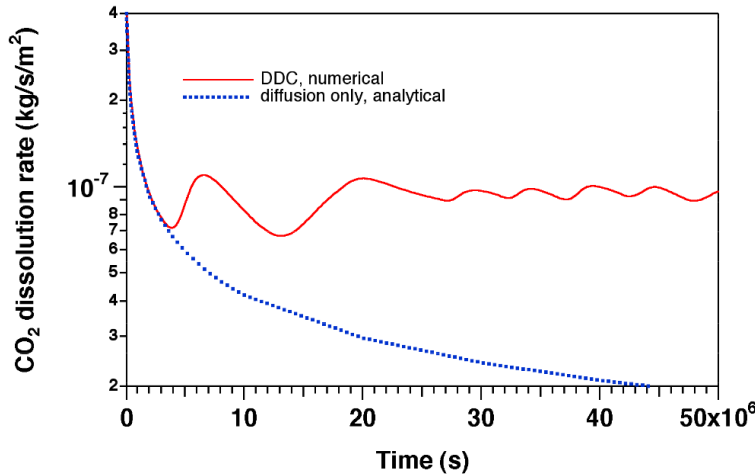


Figure 4.2: *Dissolution rate for pure dissolution (blue) and numerically found dissolution rate due to convective mixing (red), adapted from [30, 28].*

dissolution rate and thereby also the trapping of $CO_2$. This motivates us to build a model that includes convective mixing.

## 4.2 Conceptual Model

Similarly to the model described in Chapter 3 we have a region with mobile $CO_2$ (Region 1) on top of the formation, with a region of residual $CO_2$

(Region 2) in the wake of the plume. Below these two regions we imagine a region with dissolved $CO_2$ (Region 3) which is located on top of the pure brine (Region 4). An illustration of the different regions is shown in Figure 4.3. The $z-$axis is taken to be normal to the aquifer with $z = 0$ at the
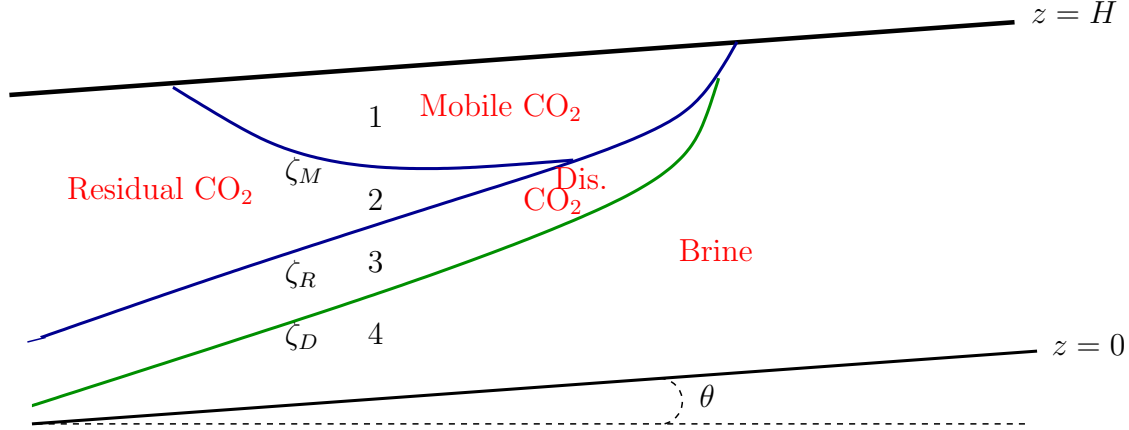


Figure 4.3: *Schematic of the different regions described in the model including solubility trapping.*

bottom layer of the aquifer and $z = H$ at the top layer. Further, the $x-$axis is taken to be in the up dip flow direction.

The interface between mobile $CO_2$ and residual and dissolved $CO_2$ is marked with $z = \zeta_M(x,t)$. The interface below the region of residual $CO_2$ is marked with $z = \zeta_R(x,t)$. Furthermore, the interface between the dissolution region and pure brine is marked with $z = \zeta_D(x,t)$. We will return to the location of the $\zeta_D$ interface later. A constraint to these interface locations is that

$$0 \leq \zeta_D \leq \zeta_R \leq \zeta_M \leq H.$$

## 4.3  Assumptions

We also apply the sharp interface approximation for this model. The saturation distribution for the $CO_2$ phase is;

$$s_c = \begin{cases} 0 & \text{for } 0 \leq z < \zeta_R, \\ s_{cr} & \text{for } \zeta_R \leq z < \zeta_M, \\ 1 - s_{br} & \text{for } \zeta_M \leq z \leq H, \end{cases}$$

where $s_{\alpha r}$ are the residual saturations for the phases $\alpha = c, b$. Notice that the brine phase is immobile in the region where the $CO_2$ phase is mobile

since $\lambda_b(s_{br}) = 0$. Similarly we see that the $CO_2$ phase is immobile where the brine phase is mobile since $\lambda_c(s_{cr}) = 0$. We also apply the vertical equilibrium approximation introduced in Chapter 3. Recall that this approximation involves neglecting vertical flow, which gave us a hydrostatic fluid pressure in the direction perpendicular to the aquifer plane.

We take the fluid properties within each of the regions to be constant and at equilibrium. Furthermore we assume equilibrium between the $CO_2$ and brine phases in each of the regions. The models presented here does not only include the effect of

In this model $CO_2$ is present as pure or dissolved $CO_2$. From Section 2.2.4 we know that when a phase is made up of several components the composition can be described in terms of the mass fraction $m_\alpha^i$, where

$$m_\alpha^i = \frac{\text{mass of the component } i \text{ in phase } \alpha}{\text{total mass in phase } \alpha} = \frac{M_\alpha^i}{\sum\limits_i M_\alpha^i}.$$

For the density we introduced the superscript $mix$ to indicate a mixture of several components in a phase, $\rho_\alpha^{mix}$. In Region 4 where there is no mixing we only have pure phase brine and the density is denoted *pure* to indicate this. The vertical density distribution will be

$$\rho_b = \begin{cases} \rho_b^{mix} & \text{if } \zeta_D \leq z \leq H, \\ \rho_b^{pure} & \text{if } 0 \leq z < \zeta_D, \end{cases} \quad \text{and} \quad \rho_c = \rho_c^{mix} \quad \text{if } 0 \leq z \leq H.$$

The interface $\zeta_D$ is defined such that all the dissolved $CO_2$ is in equilibrium in the region between $\zeta_D$ and $\zeta_R$. We assume that in regions where both phases coexist, the concentrations reach equilibrium values instantaneously. Moreover, we have that there is no $CO_2$ component in Region 4. Hence we have that

$$m_\alpha^i = \begin{cases} m_\alpha^{i,eq} & \text{if} & \zeta_D \leq z \leq H, \\ 1 & \text{if } \alpha = i = b \text{ and} & 0 \leq z < \zeta_D, \\ 0 & & \text{else,} \end{cases}$$

where the superscript *eq* indicates that the mass fraction is equal to the equilibrium constant, that is the solubility limit.

## Dissolution Rate

In the absence of convective mixing we have that dissolved $CO_2$ is produced when pure brine moves into a region of $CO_2$ (or opposite) when $\zeta_R = \zeta_D$. Once these interfaces are separated, convective mixing will occur at a rate presumed known.

As mentioned above, convective mixing accelerates the dissolution process. Both the process of diffusion and convective mixing has been studied in several works [10, 22, 30, 31]. These studies has focused on analyzing the onset time for convective mixing and the thickness of the diffusive boundary layer at that time. From high resolution simulations Pau et al. in [28] obtained a $CO_2$ dissolution rate due to convective mixing equal to $1.0 \cdot 10^{-7} \mathrm{kg/s/m^2}$. This can be seen in Figure 4.2. By comparing this $CO_2$ mass transfer rate with the analytical solution for diffusion only, they deduce a onset time for convective mixing of $4.0 \cdot 10^6 \mathrm{s}$ ($\approx 46$ days). Accordingly, the process of diffusion and convective mixing will start practically instantaneously relative to the characteristic time scales of plume migration. This results in some important assumptions;

  i) We assume that the onset time of instability for convective mixing to begin is short compared to other post- injection processes.

 ii) Once this onset time has passed, we assume that the dissolution process is linear and can be approximated by a constant dissolution rate. The dissolution rate is assumed to be constant and independent of time.

iii) Effects from the bottom layer of the aquifer that would eventually reduce the dissolution rate are neglected.

 iv) When there is no $CO_2$ available to dissolve into brine, the dissolution rate is set equal to zero.

To sum up, we have that

$$C_R(x) = \begin{cases} C & \text{if } \zeta_M < H, \\ 0 & \text{if } \zeta_D = 0 \end{cases} \qquad \text{or} \qquad \zeta_D = \zeta_R = \zeta_M = H.$$

# 4.4   Mathematical Model

In this section a mathematical model that includes both residual and solubility trapping will be described. As mentioned the idea is to upscale the model describing the mass transfer in the system.

### 4.4.1 Governing Equations

First we do a calculation of the total mass $m^i$ for the $CO_2$ and the brine components at the fine scale. Both components are present in both phases, so that

$$m^i = \phi \sum_\alpha \rho^i_\alpha s_\alpha,$$

where the total mass flux for each component is

$$f^i = \sum_\alpha \rho^i_\alpha u_\alpha.$$

Then, the Mass Conservation Equation for each component reads

$$\frac{\partial m^i}{\partial t} + \frac{\partial f^i}{\partial x} = 0.$$

Next, we upscale this equation to the coarse scale by integrating vertically over the aquifer considering a cross-section of the aquifer as the one shown in Figure 4.4
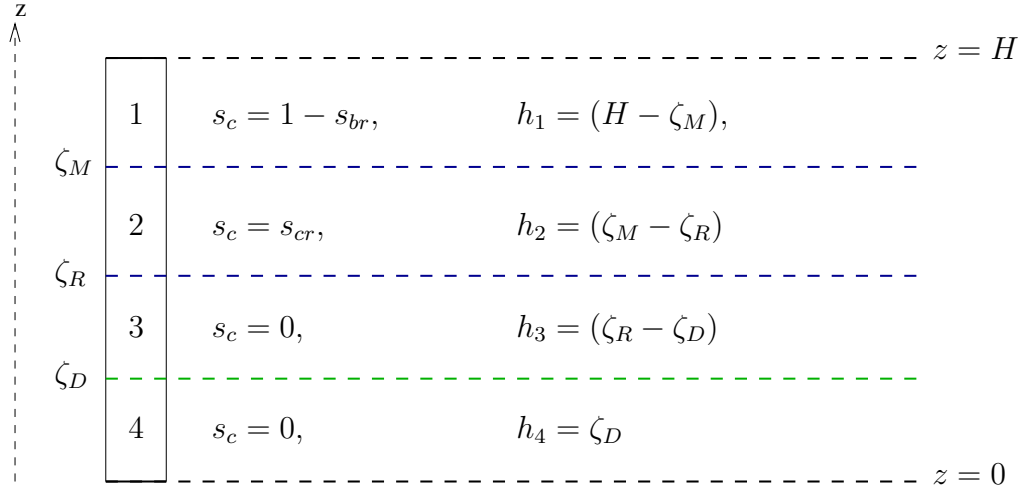


Figure 4.4: *Vertical cross section of the aquifer, with parameter values for each region.*

We have that the upscaled total mass of component $i$ per unit area in phase

$\alpha$ is expressed as

$$
\begin{aligned}
M^c &= \phi\left[\rho_b^{mix}m_b^{c,\mathrm{eq}}\Big((\zeta_R-\zeta_D)+(1-S_{cr})(\zeta_M-\zeta_R)+S_{br}(H-\zeta_M)\Big)\right] \\
&\quad + \phi\left[\rho_c^{mix}m_c^{c,\mathrm{eq}}\Big(S_{cr}(\zeta_M-\zeta_R)+(1-S_{br})(H-\zeta_M)\Big)\right] \\
M^b &= \phi\left[\rho_b^{mix}m_b^{b,\mathrm{eq}}\Big((\zeta_R-\zeta_D)+(1-S_{cr})(\zeta_M-\zeta_R)+S_{br}(H-\zeta_M)\Big)+\rho_b^{pure}\zeta_D\right] \\
&\quad + \phi\left[\rho_c^{mix}m_c^{b,\mathrm{eq}}\Big(S_{cr}(\zeta_M-\zeta_R)+(1-S_{br})(H-\zeta_M)\Big)\right]
\end{aligned}
\tag{4.1}
$$

This gives us the upscaled mass conservation equations

$$
\frac{\partial M^i}{\partial t}+\frac{\partial F^i}{\partial x} = 0, \tag{4.2}
$$

where $i=c,b$. Here the upscaled flux of each component $i$ is

$$
F^i = \sum_\alpha \int_0^H \rho_\alpha^i u_\alpha, \tag{4.3}
$$

where $u_\alpha$ is the fine scale Darcy velocity of phase $\alpha$ within the different regions. Region 4 is the only region where the $CO_2$ is mobile and $u_b = 0$. From Darcy's law the phase Darcy velocities in the x-direction are

$$
u_\alpha = -k\lambda_\alpha\left(\frac{\partial p_\alpha}{\partial x}-\rho_\alpha g\sin\theta\right).
$$

To find expressions for the Darcy velocities in the different regions we need fine scale expressions for the pressures in each region. We have assumed that the pressure distribution is hydrostatic and we choose the pressure of datum to be at the bottom of the aquifer. Then the fine scale pressure for the brine phase is

$$
p_b(x;z) = \begin{cases} P - g\cos\theta\rho_b^{pure}z, & \text{if } 0\le z\le\zeta_D, \\ p_b(x;\zeta_D)-g\cos\theta\rho_b^{mix}(z-\zeta_D), & \text{if } \zeta_D < z\le H, \end{cases}
$$

where $P = p_b(x;0)$. Similarly, for the pressure for the $CO_2$ phase we obtain

$$
p_c(x;z) = p_c(x;\zeta_M)-g\cos\theta\rho_c^{mix}(z-\zeta_M).
$$

Usually the datum pressure for the $CO_2$ phase is connected to the brine phase pressure through the entry capillary pressure $p_{entry}^{cap}$;

$$
p_c(x;\zeta_M) = p_b(x;\zeta_M)+p_{entry}^{cap}.
$$

We neglect $p_{entry}^{cap}$ and we have that $p_c(x; \zeta_M) = p_b(x; \zeta_M)$. That is,

$$p_c(x; z) = P - g\cos\theta \left( \rho_b^{pure}\zeta_D + \rho_b^{mix}(\zeta_M - \zeta_D) + \rho_c^{mix}(z - \zeta_M) \right).$$

Taking $\lambda_{\alpha j}$ as mobilities in the 4 regions ($j = 1, 2, 3, 4$), the Darcy velocities are given by

$$u_b = \begin{cases} -k\lambda_{b4}\left(\dfrac{\partial P}{\partial x} - g\rho_b^{pure}\sin\theta\right), & \text{if } 0 \leq z \leq \zeta_D, \\[2ex] -k\lambda_{b3}\left(\dfrac{\partial P}{\partial x} - g\cos\theta\dfrac{\partial\zeta_D}{\partial x}(\rho_b^{pure} - \rho_b^{mix}) - g\rho_b^{mix}\sin\theta\right), & \text{if } \zeta_D < z \leq \zeta_R, \\[2ex] -k\lambda_{b2}\left(\dfrac{\partial P}{\partial x} - g\cos\theta\dfrac{\partial\zeta_D}{\partial x}(\rho_b^{pure} - \rho_b^{mix}) - g\rho_b^{mix}\sin\theta\right), & \text{if } \zeta_R < z \leq \zeta_M, \end{cases}$$

and as mentioned $u_b = 0$ in region 4. The $CO_2$ phase is only mobile when $\zeta_M \leq z \leq H$ and then we have that

$$u_c = -k\lambda_{c1}\left(\frac{\partial P}{\partial x} - g\cos\theta\left(\frac{\partial\zeta_D}{\partial x}(\rho_b^{pure} - \rho_b^{mix}) + \frac{\partial\zeta_M}{\partial x}(\rho_b^{mix} - \rho_c^{mix})\right) - g\rho_c^{pure}\sin\theta\right).$$

After substituting the expressions for the Darcy velocities into equation (4.2) we obtain a system of two equations with 4 unknowns; the interfaces $\zeta_D(x, t)$, $\zeta_R(x, t)$, $\zeta_M(x, t)$ and the pressure of datum $P = p(x; 0)$. Thus we need to add additional closure equations to solve the system.

## 4.4.2 Modeling Choices

To obtain equations to close our system we follow the suggestions by Gasda et al. in [12]. First we consider dissolution by component transfer within the system. We consider the mass of $CO_2$ dissolved in the brine

$$M_b^c = \phi\rho_b^{mix}m_b^{c,eq}\left((\zeta_R - \zeta_D) + (1 - S_{cr})(\zeta_M - \zeta_R) + S_{br}(H - \zeta_M)\right). \tag{4.4}$$

This variable is not a conserved quantity, but satisfies a transport relation of the form

$$\frac{\partial M_b^c}{\partial t} + \frac{\partial F_b^c}{\partial x} = C_R, \tag{4.5}$$

where $C_R$ is the mass production rate of dissolved $CO_2$ and

$$F_b^c = \rho_b^{mix}m_b^{c,eq}\int_{\zeta_D}^{\zeta_M} u_b \, \mathrm{d}z. \tag{4.6}$$

This transport equation (4.5) holds under the constraint that $0 \leq \zeta_D \leq \zeta_R$. To fulfill the constraint we solve (4.5) for $\frac{\partial \zeta_D}{\partial t}$ and we get that

$$\frac{\partial \zeta_D}{\partial t} = \frac{1}{\phi \rho_b^{mix} m_b^{c,\mathrm{eq}}} \left( -C_R + \frac{\partial F_b^c}{\partial x} \right) + S_{cr} \frac{\partial \zeta_R}{\partial t} + (1 - S_{cr} - S_{br}) \frac{\partial \zeta_M}{\partial t} \equiv D_1. \tag{4.7}$$

If $\zeta_D = \zeta_R$, this means that there is no region of dissolved $CO_2$, thus the height of the interface $\zeta_D$ can only decrease or change like $\zeta_R$. In the opposite case, when $\zeta_D = 0$, $CO_2$ has dissolved into pure brine all the way to the bottom of the aquifer, thus no more $CO_2$ can dissolve into brine. The height of the surface can only stay zero or increase. If $\zeta_D$ does not interact with any of the other surfaces, the expression (4.7) yields. To sum up

$$\frac{\partial \zeta_D}{\partial t} = \begin{cases} \min(D1, \frac{\partial \zeta_R}{\partial t}), & \text{if } \zeta_R = \zeta_D, \\ D1, & \text{if } 0 < \zeta_D < \zeta_R, \\ \max(D1, 0), & \text{if } \zeta_D = 0. \end{cases} \tag{4.8}$$

Secondly we consider hysteresis to obtain the second modeling equation. Whenever $\zeta_R < \zeta_M$, we assume that all the $CO_2$ dissolves into the brine originates from the region of residual $CO_2$. This is equivalent to say that the mobile $CO_2$ is conserved and we have that,

$$\phi(1 - s_{cr} - s_{br}) \frac{\partial \zeta_M}{\partial t} + \frac{\partial}{\partial x} \int_{\zeta_M}^{H} u_c \mathrm{d}z = 0. \tag{4.9}$$

The mobile $CO_2$ is then conserved under the constraint that $\zeta_R < \zeta_M < H$. To fulfill this constraint we write

$$\frac{\partial \zeta_M}{\partial t} = \frac{-1}{\phi(1 - s_{cr} - s_{br})} \frac{\partial}{\partial x} \int_{\zeta_M}^{H} u_c \mathrm{d}z \equiv D_2. \tag{4.10}$$

When $\zeta_M = H$, the height $\zeta_M$ either decreases or stays unchanged. In the opposite case, when $\zeta_M = \zeta_R$ the interface $\zeta_M$ can only decrease or change like $\zeta_R$. If the interface $\zeta_M$ does not interact with any of the other interfaces, $\zeta_M$ changes like (4.10). To sum up

$$\frac{\partial \zeta_M}{\partial t} = \begin{cases} \min(D2, 0), & \text{if } \zeta_M = H, \\ D2, & \text{if } \zeta_R < \zeta_M < H, \\ \max(D2, \frac{\partial \zeta_R}{\partial t}), & \text{if } \zeta_M = \zeta_R. \end{cases} \tag{4.11}$$

Equations (4.8) and (4.11) provides us with two equations that close the system.

### 4.4.3 Instability Remark

We have now developed a system of coarse scale equations that models the dissolution process. On the fine scale convective mixing is considered as a unstable and chaotic process. If we consider a region where we only have pure brine, i.e. $\zeta_D = \zeta_R = \zeta_M = H$, the model simplifies to the model presented in Chapter 3. However, the density difference $\Delta\rho = \rho_b - \rho_c$ from the model in Chapter 3 is positive unlike the density difference in this model $\Delta\rho = \rho_b^{mix} - \rho_b^{pure}$ which is negative. This sign difference prevents the second order term from working as a smoothening term in this model.

In our coarse scale model we make no effort at dampening the instabilities from the fine scale and the coarse scale model is also instable. Convective mixing is therefore a fascinating example of preserving the unstable characteristic of the fine scale equations in the coarse scale model. In [25] Celia and Nordbotten suggest ways of dealing with this in practice and we will return to this in the model application in Chapter 6.

### 4.4.4 Pressure Equation

To obtain an equation for the unknown datum pressure we consider the volume

$$\{ \text{ pure } CO_2 \} \ + \ \{ CO_2 \text{ dissolved in brine} \} \ + \ \{ \text{ pure brine } \}.$$

We note that we have pure $CO_2$, $CO_2$ dissolved in brine and pure brine distributed in our different regions as follows:

| | | | | |
|---|---|---|---|---|
| 1 | pure $CO_2$ (mobile), | dissolved $CO_2$ | $H$ | $\{ h_1 = H - \zeta_M$ |
| 2 | pure $CO_2$ (residual), | dissolved $CO_2$ | $\zeta_M$ | $\{ h_2 = \zeta_M - \zeta_R$ |
| 3 | | dissolved $CO_2$ | $\zeta_R$ | $\{ h_3 = \zeta_R - \zeta_D$ |
| 4 | pure brine | | $\zeta_D$ | $\{ h_4 = \zeta_D$ |
| | | | $0$ | |

If we look at a narrow cross section of the aquifer the sum of these three volumes equals the total volume of this cross section, that is $H$. Expressions

for these three volumes can be found by combining the three expressions for the masses $M^b$, $M^c$ and $M_b^c$ that we already have. An expression for the volume of the pure phase $CO_2$ is obtained by subtracting the expression for the dissolved $CO_2$ from the total $CO_2$ component

$$
\begin{aligned}
V_c^c &= \frac{M_c^c}{\rho_c^{mix}m_c^{c,\text{eq}}} \\
&= \frac{1}{\rho_c^{mix}m_c^{c,\text{eq}}}(M^c - M_b^c) = \phi\left(s_{cr}h_2 + (1 - s_{br})h_1\right).
\end{aligned}
\tag{4.12}
$$

Dividing the mass of dissolved $CO_2$ by the mixture density we obtain an expression for the volume of the dissolved $CO_2$,

$$
\begin{aligned}
V_b^c &= \frac{M_b^c}{\rho_b^{mix}m_b^{c,\text{eq}}} \\
&= \phi\left(h_3 + (1 - s_{cr})h_2 + s_{br}h_1\right).
\end{aligned}
\tag{4.13}
$$

For pure brine, we can achieve an expression by subtracting the following terms from the total brine component

$$
\begin{aligned}
V_b^b &= \frac{M_b^b}{\rho_b^{pure}} \\
&= \frac{1}{\rho_b^{pure}}\left(M^b - \frac{m_c^{b,\text{eq}}}{m_c^{c,\text{eq}}}(M^c - M_b^c) - \frac{m_b^{b,\text{eq}}}{m_b^{c,\text{eq}}}M_b^c\right) = \phi h_4.
\end{aligned}
\tag{4.14}
$$

We add these volumes and obtain

$$
V_c^c + V_b^c + V_b^b = \phi H \equiv V,
$$

which is the total volume per unit area in the aquifer.

Next, we add the Mass Conservation equations (4.2) and (4.5) to get the total volume. We do this by,

$$
A_1\left(\frac{\partial M^b}{\partial t} + \frac{\partial F^b}{\partial x}\right) + A_2\left(\frac{\partial M^c}{\partial t} + \frac{\partial F^c}{\partial x}\right) + A_3\left(\frac{\partial M_b^c}{\partial t} + \frac{\partial F_b^c}{\partial x}\right) = A_3 C_R,
\tag{4.15}
$$

where the coefficients are

$$
A_1 = \frac{1}{\rho_b^{pure}},
$$

$$
A_2 = \frac{1}{\rho_c^{mix}m_c^{c,\text{eq}}} - \frac{m_c^{b,\text{eq}}}{\rho_b^{pure}m_c^{c,\text{eq}}},
$$

$$
A_3 = \frac{1}{\rho_b^{mix}m_b^{c,\text{eq}}} - \frac{1}{\rho_c^{mix}m_c^{c,\text{eq}}} + \frac{m_c^{b,\text{eq}}}{\rho_b^{pure}m_c^{c,\text{eq}}} - \frac{m_b^{b,\text{eq}}}{\rho_b^{pure}m_b^{c,\text{eq}}}.
$$

We know that the thicknesses of the regions must fulfill the relation

$$h_1 + h_2 + h_3 + h_4 = H.$$

In equation (4.15) we for the time derivative obtain

$$\phi \frac{\partial}{\partial t} (h_1 + h_2 + h_3 + h_4) = \phi \frac{\partial}{\partial t} H \equiv \frac{\partial}{\partial t} V = 0.$$

This results in an equation of the form

$$\underbrace{\frac{\partial H}{\partial t}}_{= 0} + \frac{\partial}{\partial x} \left( A_1 F^b + A_2 F^c + A_3 F_b^c \right) = A_3 C_R. \tag{4.16}$$

By integration we find that

$$A_1 F^b + A_2 F^c + A_3 F_b^c = A_3 \int_{\tilde{x}}^{x} C_R \mathrm{d}x' + A_1 F^b|_{x=\tilde{x}} + A_2 F^c|_{x=\tilde{x}} + A_3 F_b^c|_{x=\tilde{x}}, \tag{4.17}$$

where $\tilde{x}$ is some boundary in our domain. If we take this boundary to be inside the initial $CO_2$ plume, we have the boundary conditions

$$F^b|_{x=\tilde{x}} = 0,$$
$$F^c|_{x=\tilde{x}} = 0,$$
$$F_b^c|_{x=\tilde{x}} = 0,$$

and we can solve the equation (4.17) for the unknown datum pressure.

The full derivation of the expression for the unknown datum pressure $P$ is presented in Appendix A. This expression is found by substituting the expressions for the upscaled flux functions into (4.17). As mentioned this is done in detail in Appendix A, and results in an expression of the form

$$\frac{\partial P}{\partial x} = p_1(\zeta_D, \zeta_R, \zeta_M) + p_2(\zeta_D, \zeta_R, \zeta_M) \frac{\partial \zeta_D}{\partial x} + p_3(\zeta_D, \zeta_R, \zeta_M) \frac{\partial \zeta_M}{\partial x}. \tag{4.18}$$

# Chapter 5

# Numerical Model

In this chapter we describe the numerical solution approach for the model developed in the previous chapter. The numerical tools and the stabilization restrictions are given. We also discuss some of the problems and challenges we have had solving this model.

## 5.1  Solution Approach

In Section 4.4.4 we gained an equation for the unknown datum pressure $P$. When considering the thicknesses of the different regions this leaves us with four unknowns: $h_1$, $h_2$, $h_3$ and $h_4$. The four equations we use to solve for these unknowns are,

$$\frac{\partial M^c}{\partial t} = -\frac{\partial F^c}{\partial x}, \tag{5.1}$$

$$\frac{\partial M^b}{\partial t} = -\frac{\partial F^b}{\partial x}, \tag{5.2}$$

$$\frac{\partial M_b^c}{\partial t} = C_R - \frac{\partial F_b^c}{\partial x}, \tag{5.3}$$

$$\frac{\partial \zeta_M}{\partial t} = \frac{-1}{\phi(1 - S_{cr} - S_{br})} \frac{\partial}{\partial x} \int_{\zeta_M}^{H} u_c \mathrm{d}z \equiv D_2. \tag{5.4}$$

We start by solving for the component masses $M^c$, $M^b$ and the mass for dissolved $CO_2$ $M_b^c$ with equations (5.1), (5.2) and (5.3). Next, we solve for $\zeta_M$ with equation (5.4) when $\zeta_R < \zeta_M$. If we have the situation that $\zeta_R = \zeta_M$ we note that we only have three unknowns. With the knowledge of $\zeta_M, M^c, M^b$ and $M_b^c$ we use the expressions for the volumes (4.12), (4.13) and (4.14) from Section 4.4.4 to get the three volumes $V_c^c$, $V_b^c$ and $V_b^b$. When

we have the volumes we can solve for the three remaining unknowns.
When $\zeta_R = \zeta_M$, that is $h_3 = 0$ we have that

$$V_b^b = \phi h_1 \qquad \Longrightarrow \qquad h_1 = \frac{V_b^b}{\phi}$$

$$V_c^c = \phi(1 - s_{br})h_4 \qquad \Longrightarrow \qquad h_4 = \frac{V_c^c}{\phi(1 - s_{br})}$$

$$V_b^c = \phi(h_2 + s_{br}h_4) \qquad \Longrightarrow \qquad h_2 = \frac{V_c^b}{\phi} - s_{br}h_4.$$

How this is done numerically will be described in the next section.

## 5.2  Numerical Approach

We start by dividing our 1D interval into a cell-centered equidistant grid
$\{x_j, t^m\}$, where the cell center locations in space and time are given by

$$x_{j+1} = x_j + \Delta x, \qquad\qquad (5.5)$$

$$t^{m+1} = t^m + \Delta t. \qquad\qquad (5.6)$$

We take $\Delta x = (x_{N+1} - x_1)/N$ where $x_1$ and $x_{N+1}$ are chosen start and end
points respectively, and $N$ are the number of cell-centers. The time step
$\Delta t$ is limited by a stabilization criteria and will be further discussed when
a discretization method is introduced. The discretization grid is illustrated
in Figure 5.1. When the component fluxes (4.3) are inserted, the two mass
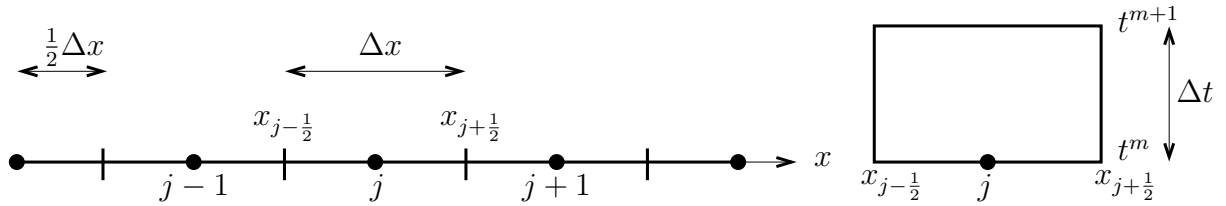


Figure 5.1: *Illustration of the grid points $j$ in the cell-centers and the cell-edges
$x_{j+\frac{1}{2}}$. To the right grid-cell number $j$ over a time step $\Delta t^{m+1}$ is drawn.*

conservation equations (5.1) and (5.2) has the same form as an advection
diffusion equation,

$$\frac{\partial M^i(\boldsymbol{h})}{\partial t} + \frac{\partial}{\partial x}\left[f_1^i(\boldsymbol{h}) + f_2^i(\boldsymbol{h})\frac{\partial h_1}{\partial x} + f_3^i(\boldsymbol{h})\frac{\partial h_4}{\partial x}\right] = 0, \qquad (5.7)$$

where $\boldsymbol{h} = [h_1 \ h_2 \ h_3 \ h_4]$. The derivation and the full expressions of the functions $f_1^i(\boldsymbol{h})$, $f_2^i(\boldsymbol{h})$ and $f_3^i(\boldsymbol{h})$ are given in Appendix A. Similarly the equation (5.3) for mass of dissolved $CO_2$ has the form

$$\frac{\partial M_b^c(\boldsymbol{h})}{\partial t} + \frac{\partial}{\partial x}\left[(f_1)_b^c(\boldsymbol{h}) + (f_2)_b^c(\boldsymbol{h})\frac{\partial h_1}{\partial x} + (f_3)_b^c(\boldsymbol{h})\frac{\partial h_4}{\partial x}\right] = C_R, \quad (5.8)$$

where the functions $(f_j)_b^c$ also are given in Appendix A. Furthermore, the equation (5.4) for conservation of the mobile $CO_2$ has the form

$$\frac{\partial \zeta_M}{\partial t} + a\frac{\partial}{\partial x}\left[g_1(\boldsymbol{\zeta}) + g_2(\boldsymbol{\zeta})\frac{\partial \zeta_D}{\partial x} + g_3(\boldsymbol{\zeta})\frac{\partial \zeta_D}{\partial x}\right] = 0, \quad (5.9)$$

where $\boldsymbol{\zeta} = [\zeta_D \ \zeta_R \ \zeta_M]$, $a$ is a constant and the derivation and the full expressions of the functions $g_1(\boldsymbol{\zeta})$, $g_2(\boldsymbol{\zeta})$ and $g_3(\boldsymbol{\zeta})$ are given in Appendix A.

If we start by looking at the equation (5.7) without the diffusion terms we have an equation of the form:

$$u_t + f(u)_x = 0, \quad (5.10)$$

which is a *Hyperbolic Conservation Law*. For equations on this form there exists several numerical methods, see e.g. [21]. Especially the methods that express local conservation within each cell is of importance. A method with local conservation is a method of the form

$$\frac{u_j^{m+1} - u_j^m}{\Delta t^{m+1}} + \frac{\phi_{j+\frac{1}{2}}^{m+\frac{1}{2}} - \phi_{j-\frac{1}{2}}^{m+\frac{1}{2}}}{\Delta x_j} = 0,$$

where $\phi_{j\pm\frac{1}{2}}^{m+\frac{1}{2}}$ denote the fluxes over the cell edges, which are approximated as

$$\phi_{j\pm\frac{1}{2}}^{m+\frac{1}{2}} \approx \frac{1}{\Delta t^{m+1}} \int\limits_{t^m}^{t^{m+1}} f(u(x_{j\pm\frac{1}{2}}, t))\mathrm{dt}.$$

A mass conservative method ensures that the amount of mass in a cell at time step $m+1$ is equal to mass in the cell at time step $m$ minus what has left the cell in the time-interval $\Delta t^{m+1}$. The different numerical methods differ on how the flux $\phi_{j\pm\frac{1}{2}}^{m+\frac{1}{2}}$ is discretized. Usually the flux over one edge is decided by the values in the two neighboring cells (two point stencil)

$$\phi_{j\pm\frac{1}{2}}^{m+\frac{1}{2}} = \begin{cases} \phi(u_j^m, u_{j\pm1}^m) & \textit{explicit method,} \\ \phi(u_j^{m+1}, u_{j\pm1}^{m+1}) & \textit{implicit method.} \end{cases}$$

We use a *Lax-Friedrichs* scheme to discretize the equations (5.1), (5.2), (5.3) and (5.4).

# 5.3   Lax-Friedrichs Method

In this section we describe the explicit form of the Lax-Friedrichs (L-F) method. The general L-F discretization scheme arises when looking at equation (5.10) with an artificial diffusion term,

$$u_t + f(u)_x - \frac{\Delta x^2}{2\Delta t} u_{xx} \;=\; 0.$$

The resulting explicit discretization scheme is:

$$u_j^{m+1} - \frac{1}{2}\left(u_{j-1}^m + u_{j+1}^m\right) + \frac{\Delta t}{2\Delta x}\left[f(u_{j+1}^m) - f(u_{j-1})\right] \;=\; 0, \qquad (5.11)$$

see i.e. [2, 21]. With the definition

$$\phi^{\text{LF}}(u_L, u_R) \;=\; \frac{1}{2}\left(f(u_L) + f(u_R) - \frac{\Delta x}{\Delta t}(u_R - u_L)\right),$$

where $u_L = u_{j-1}, u_j$ and $u_R = u_j, u_{j+1}$ for $\phi_{j-\frac{1}{2}}^{m+\frac{1}{2}}$ and $\phi_{j+\frac{1}{2}}^{m+\frac{1}{2}}$ respectively, the L-F scheme is on local conservation form. We will return to a discussion of the stability of this system later.

## 5.3.1   Resulting Difference Equation

In addition to using the L-F method to discretize the advection term in (5.7), we discretize the diffusion terms in the following manner,

$$\frac{\partial}{\partial x}\left(f(\boldsymbol{h})\frac{\partial h}{\partial x}\right) \;=\; \frac{f_{j+1/2}^m(h_{j+1}^m - h_j^m) + f_{j-1/2}^m(h_{j-1}^m - h_j^m)}{\Delta x^2},$$

where

$$f_{j\pm 1/2}^m \;=\; \tfrac{1}{2}\left(f(\boldsymbol{h}_j^m) + f(\boldsymbol{h}_{j\pm 1}^m)\right).$$

The obtained difference equations are

$$[M^i]_j^{m+1} \;=\; \frac{1}{2}\left([M^i]_{j-1}^m + [M^i]_{j+1}^m\right) - \frac{\Delta t}{2\Delta x}\left(f_1^i(\boldsymbol{h}_{j+1}^m) - f_1^i(\boldsymbol{h}_{j-1}^m)\right) -$$

$$\frac{\Delta t}{\Delta x^2}\Big([f_2^i]_{j+1/2}^m([h_1]_{j+1}^m - [h_1]_j^m) + [f_2^i]_{j-1/2}^m([h_1]_{j-1}^m - [h_1]_j^m) -$$

$$[f_3^i]_{j+1/2}^m([h_4]_{j+1}^m - [h_4]_j^m) + [f_3^i]_{j-1/2}^m([h_1]_{j-1}^m - [h_1]_j^m)\Big)$$

$$[M_b^c]_j^{m+1} \;=\; \frac{1}{2}\left([M_b^c]_{j-1}^m + [M_b^c]_{j+1}^m\right) - \frac{\Delta t}{2\Delta x}\left((f_1)_b^c(\boldsymbol{h}_{j+1}^m) - (f_1)_b^c(\boldsymbol{h}_{j-1}^m)\right) -$$

$$\frac{\Delta t}{\Delta x^2}\Big([(f_2)_b^c]_{j+1/2}^m([h_1]_{j+1}^m - [h_1]_j^m) + [(f_2)_b^c]_{j-1/2}^m([h_1]_{j-1}^m - [h_1]_j^m) -$$

$$[(f_3)_b^c]_{j+1/2}^m([h_4]_{j+1}^m - [h_4]_j^m) + [(f_3)_b^c]_{j-1/2}^m([h_1]_{j-1}^m - [h_1]_j^m)\Big) + \Delta t C_R.$$

Similarly we discretize the equation for the interface $\zeta_M$ as

$$
\begin{aligned}
[\zeta_M]_j^{m+1} &= \frac{1}{2}\left([\zeta_M]_{j-1}^m + [\zeta_M]_{j+1}^m\right) - \frac{\Delta t}{2\Delta x}\left(g_1(\boldsymbol{\zeta}_{j+1}^m) - g_1(\boldsymbol{\zeta}_{j-1}^m)\right) - \\
&\quad \frac{\Delta t}{\Delta x^2}\Big([g_2]_{j+1/2}^m([\zeta_D]_{j+1}^m - [\zeta_D]_j^m) + [g_2]_{j-1/2}^m([\zeta_D]_{j-1}^m - [\zeta_D]_j^m) - \\
&\quad [g_3]_{j+1/2}^m([\zeta_M]_{j+1}^m - [\zeta_M]_j^m) + [g_3]_{j-1/2}^m([\zeta_D]_{j-1}^m - [\zeta_D]_j^m)\Big).
\end{aligned}
$$

This approach updates the component masses $M^i$ and the mass of dissolved $CO_2$ by using the thicknesses of the regions from the previous time step. When the masses are updated we use these values together with the new value for $\zeta_M$ to update $\zeta_R$ and $\zeta_D$ with the volume expressions (4.12),(4.13) and (4.14) from Chapter 4.

## 5.3.2 Stability and Monotonicity

To ensure that the numerical solution of the difference equation actually converges to the true solution of the differential equation it approximates, it needs to satisfy some conditions. It has been shown that a necessary stability condition for this convergence is;

**Condition 5.1.** *The domain of dependence of the finite difference method used should include the domain of dependence of the differential equation it is approximating, at least in the limit as $\Delta t$, $\Delta x \to 0$.*
*Mathematically this has been shown [21] that for the equation $u_t + f(u)_x = 0$ this can be expressed as:*

$$
\frac{\Delta t}{\Delta x}||f'(u)||_{L^\infty} \le 1.
$$

Condition 5.1 is known as the *Courant-Friedrichs-Lewy(CFL)-condition*. The domain of dependence for the point $(x, t)$ when looking at the equation $u_t + f(u)_x = 0$ is defined as the point $\xi = x - f(u)t$ on the $x$-axis. If the CFL-condition is violated then there are points $\xi$ in the true domain of dependence that are not in the numerical domain of dependence. Changing the value of the initial data at $\xi$ would thus have an effect on the true solution but not on the numerical solution, and hence the numerical solution would not converge to the true solution for all initial data. The stability and convergence of the numerical solution can be demonstrated when the CFL-condition is fulfilled [2, 21].

Another useful property of a numerical method is called *monotonicity*. If a method is monotone it automatically fulfills the *entropy condition*. This condition will not be further discussed here but is a important condition that ensures that the correct solution is uniquely determined, for details see [21]. We will now make sure that the explicit L-F method is monotone.

An explicit method can be written on the form $\boldsymbol{u}^{m+1} = \boldsymbol{G}(\boldsymbol{u}^m)$, where

$$\boldsymbol{u}^m = \begin{bmatrix} \cdots, & u_{j-1}^m, & u_i^m, & u_{j+1}^m, & \cdots \end{bmatrix}^{\mathrm{T}},$$

is a vector that contains the solution in all the cells at time step $t^m$ [2].

**Definition 5.1.** *An explicit method is called monotone if*

$$\boldsymbol{u} - \boldsymbol{v} \geq \boldsymbol{0} \quad \Longrightarrow \quad \boldsymbol{G}(\boldsymbol{u}) - \boldsymbol{G}(\boldsymbol{v}) \geq \boldsymbol{0}.$$

For an explicit method it holds to check if the Jacobi-matrix $\boldsymbol{G}'(\boldsymbol{u}) \geq \boldsymbol{0}$. If this is fulfilled then the method is said to be monotone [2]. An L-F explicit method can be written on the form $\boldsymbol{u}^{m+1} = \boldsymbol{G}(\boldsymbol{u}^m)$, where:

$$G_j(\boldsymbol{u}) = \tfrac{1}{2}(u_{j-1} + u_{j+1}) - \tfrac{\Delta t}{2\Delta x}\left(f(u_{j+1}) - f(u_{j-1})\right).$$

The Jacobian-matrix $\boldsymbol{G}'(\boldsymbol{u}) \geq \boldsymbol{0}$ if

$$\frac{\partial G_j}{\partial u_j} = \qquad 0, \qquad \checkmark \tag{5.12}$$

$$\frac{\partial G_j}{\partial u_{j\pm 1}} = \tfrac{1}{2}(1 \mp \tfrac{\Delta t}{\Delta x}f'(u_{j\pm 1})) \quad \text{is not positive if } \Delta t \leq \frac{\Delta x}{||f'||_{L^\infty}}. \tag{5.13}$$

We recognize this condition as the CFL-condition. We have that the explicit L-F method is stable and monotone if the CFL-condition is satisfied. This condition gives us a restriction on the time step $\Delta t$. In order to have a stable method for our equations (5.1), (5.2) and (5.4) we must also consider restrictions due to the diffusion term. This diffusion term is also discretized explicitly and has a more strict stability condition than the CFL-condition:

$$\Delta t \leq \frac{\Delta x^2}{||f'(u)||_{L^\infty}}.$$

## 5.4   Problems and Challenges

In this section some of the problems and challenges we have met during the process of solving this model numerically.

### 5.4.1 Difficult Solution Approach

Our first solution approach to this model involved solving for the interfaces directly, without solving for the masses first. First we obtain a pressure equation in a manner similar to the one in Section 4.4.4. Next, we by substitute the expressions for the masses $M^c$, $M^b$ and $M_b^c$ into the mass conservation equations. From this we get a system of equations that can be expressed as

$$\boldsymbol{A}[\tfrac{\partial \zeta_D}{\partial t} \quad \tfrac{\partial \zeta_R}{\partial t} \quad \tfrac{\partial \zeta_M}{\partial t}]^{\mathrm{T}} \quad = \quad \boldsymbol{b},$$

where $\boldsymbol{A}$ is a 3x3 matrix with constant elements and $\boldsymbol{b}$ is a vector containing the flux terms and other terms not involving the $\partial/\partial t$ terms. If we multiply with $\boldsymbol{A}^{-1}$ on both sides of the expression we get the equation

$$[\tfrac{\partial \zeta_D}{\partial t} \quad \tfrac{\partial \zeta_R}{\partial t} \quad \tfrac{\partial \zeta_M}{\partial t}]^{\mathrm{T}} \quad = \quad \boldsymbol{A}^{-1}\boldsymbol{b}.$$

From this equation system we can solve for the three interfaces $\zeta_D$, $\zeta_R$ and $\zeta_M$ explicitly forward in time.

However, this solution approach involves several situations where the interface-location constraint must be considered. This means that two or more of the interfaces interact and we have constraints on the modeling equations. When we take this into consideration we end up with a complicated system, with many possible places to do something wrong. Therefore, the approach described in the previous sections was chosen instead.

### 5.4.2 Volume Correction

When we update the component masses and the mass of dissolved $CO_2$ numerically, the associated volumes will not always add up exactly to the analytical volume of each cell. We know that the total volume per unit area is

$$V = \phi H.$$

To ensure us that we solve for the region thicknesses from a numerical volume that corresponds to the actual volume of each cell, we scale the numerical obtained volumes in the following manner

$$\left[\tilde{V}_c^c\right]_j \quad = \quad [V_c^c]_j \frac{V}{([V_c^c]_j + [V_b^c]_j + [V_b^b]_j)},$$

$$\left[\tilde{V}_b^c\right]_j \quad = \quad [V_b^c]_j \frac{V}{([V_c^c]_j + [V_b^c]_j + [V_b^b]_j)},$$

$$\left[\tilde{V}_b^b\right]_j \quad = \quad [V_b^b]_j \frac{V}{([V_c^c]_j + [V_b^c]_j + [V_b^b]_j)}.$$

We use these scaled volumes $\tilde{V}$ to update the region thicknesses as described in Section 5.1.

To minimize the volume error in the next time step we find the difference between the numerical volume in each cell and the actual volume in that cell

$$R_j = [V_c^c]_j + [V_b^c]_j + [V_b^b]_j - V. \qquad (5.14)$$

We add this correction $R_j$ into the pressure equation obtained in Section 4.4.4 for each time step,

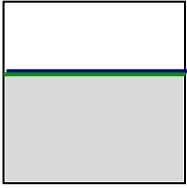$$A_1 F^b + A_2 F^c + A_3 F_b^c = A_3 C_R(x - \tilde{x}) + -\frac{R_j(x - \tilde{x})}{\Delta t}.$$

This correction ensures us that the obtained datum pressure satisfies the volume constraint.

### 5.4.3 Equation Constraints

Since the transport equation (4.5) must fulfill the relation $0 \leq \zeta_D \leq \zeta_R$, we have the limit cases (I) and (II) when $\zeta_R = \zeta_M$:
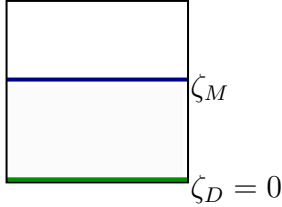


(I)  Limit case: $0 = \zeta_D < \zeta_M \leq H$, mobile $CO_2$ above dissolved $CO_2$.

(II)  Limit case: $0 < \zeta_D = \zeta_M \leq H$, no dissolved $CO_2$, mobile $CO_2$ above brine.

In limit case (I) we have that $\zeta_D = 0$ and this corresponds to no pure brine. In this situation we must be careful to not dissolve $CO_2$ below the bottom of the aquifer. If to much $CO_2$ has dissolved in the brine, we have that $\zeta_D = h_1 < 0$. If this is the case this means that we must decrease the mass of dissolved $CO_2$ $M_b^c$ such that $h_1 = 0$. This is done by considering the volume of pure brine $V_b^b$, and finding the mass $M_b^c$ that corresponds to $V_b^b = 0$,

$$V_b^b = 0 \iff M_b^c = \frac{\frac{m_c^{b,eq}}{m_c^{c,eq}} M^c - M^b}{\frac{m_c^{b,eq}}{m_c^{c,eq}} - \frac{m_b^{b,eq}}{m_b^{c,c}}}.$$

This reduces the mass of dissolved $CO_2$ such that $h_1 = 0$. The volumes $V_c^b$ and $V_c^c$ will also change as a consequence of the reduced mass $M_b^c$.

In limit case (II) we have no dissolution region and pure brine below mobile $CO_2$. If we from the updated masses get values such that $\zeta_D > \zeta_M$ ($h_2 < 0$) it means that we must dissolve in more $CO_2$ to fulfill the constraint $0 \leq \zeta_D \leq \zeta_M$. To find this increased mass $M_b^c$ we set

$$h_2 = 0 \quad \Leftrightarrow \quad M_c^b = \frac{s_{br}\rho_b^{mix}m_b^{c,\mathrm{eq}}}{(1 - s_{br}) + s_{br}\rho_b^{mix}m_b^{c,\mathrm{eq}}}M^c.$$

From this increased $M_b^c$ value we get new values for the volumes $V_c^c$, $V_b^c$ and $V_b^b$.

# Chapter 6

# Model Application and Results

In this chapter we describe the deep saline aquifer and its related parameters the model presented in Chapter 4 is applied to. We look at the plume migration and especially the influence the value of the dissolution rate has on the plume velocity. The numerical results are presented and discussed.

## 6.1   Model Problem

We apply the model in Chapter 4 to the benchmark study proposed by Dahle et al. in [9]. This study features a relatively simple geological storage problem and is designed to highlight important questions around the long-term fate of the injected $CO_2$. We look at a sloping saline aquifer with constant thickness $H$. Both the top and bottom of the aquifer are assumed to be impermeable rocks. When it comes to the side boundaries we assume that they are open to flow along the entire extent of the domain. For simplicity we assume that injection has stopped and that we initially have a rectangular $CO_2$ plume of width $b$ and height $H$. This initial plume is located at the interval $[x_1 \ x_2]$, see Figure 6.1.

This initial condition represents a finite release of $CO_2$ and is a piecewise constant initial data as we mentioned in Chapter 3. We take this condition to be:

$$\zeta_D(x,0) = \zeta_R(x,0) = \zeta_M(x,0) = \begin{cases} 0 & \text{if } x_1 < x < x_2, \\ H & \text{else.} \end{cases}$$

We assume homogeneous permeability and constant fluid properties listed in Table 6.2. The relative permeability functions $k_{rb}(s_c)$ and $k_{rc}(s_c)$ are given by the simple power law expressions by Brooks and Corey that we defined in
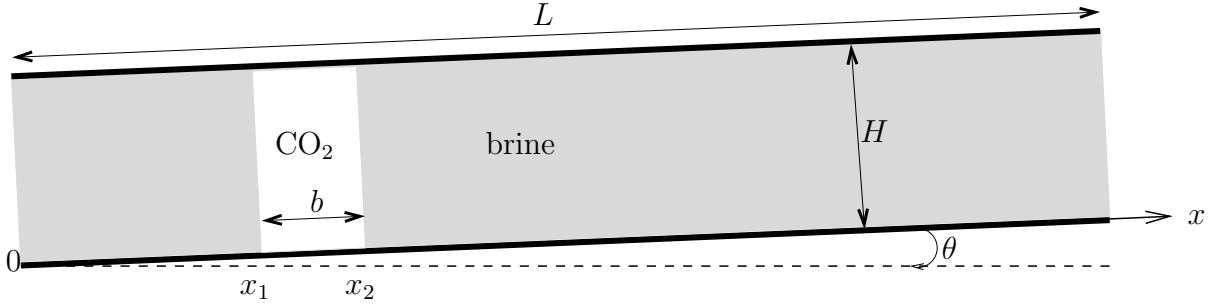
Figure 6.1: *Sketch over the initial situation in the saline aquifer we are modeling $CO_2$ migration in. The initial $CO_2$ plume are marked in white and have width b and height $H$. The lateral extent we look at is at a length $L$.*

Chapter 2. Here hysteresis is included in the relative permeability functions and we have

$$k_{rc} = 0.4(1 - s_{bn}^2)(1 - s_{bn})^2 - C, \qquad (6.1)$$

$$k_{rb} = s_{bn}^4, \qquad (6.2)$$

$$s_{bn} = \frac{s_b - s_{br}}{1 - s_{br}},$$

where $C$ is a constant such that $k_{rc} = 0$ when $s_c = s_{cr}$ ($\sim 0.25$ for the residual saturations given in Table 6.2).

We assume line symmetry along the dip direction. Since we look at the migration in 1D we assume that the domain is symmetric along the center axis of the domain perpendicular to the dip angle. As mentioned we use an equidistant grid where each cell has width $\Delta x$ along the dip direction.

## 6.2   Model Application

We apply the model developed in Chapter 4 to the problem described in the previous section. We want to study the effect of dissolution when we include convective mixing. The effect of residual trapping is neglected in this study, and set $\zeta_R = \zeta_M$ ($h_2 = 0$). The equation for the sum of the thicknesses ($h_1 + h_3 + h_4 = H$) is used to find a pressure equation like described in Section 4.4.4. The three mass conservation equations are used to update the masses $M^c$, $M^b$, $M_b^c$ in each time step. From these updated masses we find the thicknesses $h_1$, $h_3$ and $h_4$ like we described in Chapter 5.

| Parameter | Symbol | Unit | Value | |
|---|---|---|---|---|
| Porosity | $\phi$ | [-] | 0.15 | |
| Height | $H$ | [m] | 50 | |
| Length | $L$ | [m] | | 150000 |
| Initial $CO_2$ plume width | $b$ | [m] | 4000 | |
| Initial $CO_2$ filled int. | $[x_1\ x_2]$ | [m] | | |
| Dip angle | $\theta$ | [-] | 2% | |
| Permeability | $k$ | [m$^2$] | $1 \cdot 10^{-13}$ | |
| Mass fraction of $CO_2$ in brine | $m_b^{c,eq}$ | [-] | 0.02 | |
| Mass fraction of brine in $CO_2$ | $m_c^{b,eq}$ | [-] | 0 | |
| Mix $CO_2$ density | $\rho_c^{mix}$ | [kg/m$^3$] | 733 | |
| Mix brine density | $\rho_b^{mix}$ | [kg/m$^3$] | 1099 | * |
| Pure brine density | $\rho_b^{pure}$ | [kg/m$^3$] | 1099 | * |
| $CO_2$ viscosity | $\mu_c$ | [kg/s m] | 0.000061 | |
| Brine viscosity | $\mu_b$ | [kg/s m] | 0.000511 | |
| Residual brine saturation | $s_{br}$ | [-] | 0.2 | |
| Residual $CO_2$ saturation | $s_{cr}$ | [-] | 0.2 | |
| Relative $CO_2$ permeability | $k_{rc}$ | [-] | | (6.1) |
| Relative brine permeability | $k_{rb}$ | [-] | | (6.2) |
| $CO_2$ dissolution rate | $C_R$ | [kg/m$^2$/s] | | |

Table 6.2: *Table over the values assigned to the saline aquifer and to the different rock and phase properties.*
*(\*)Note that we set $\rho_b^{mix} = \rho_b^{pure}$. We remember the remark on instability from section 4.4.3. The unstable term is proportional to $(\rho_b^{mix} - \rho_b^{pure})$, which usually is on the order of a few [kg/m$^3$] [25]. In principle it is this term that drives the instabilities on the fine scale. However, one may consider this density difference as insignificant on the coarse scale and thus avoid the problem with an unstable coarse scale model. Modeling of the impact of convective mixing will then relie on the dissolution rate $C_R$. This will not be further discussed here.*

## 6.2.1 Plume Migration

The travel distance and the corresponding migration time are important temporal and spatial scales for $CO_2$ sequestration. We look at migration differences when we

A) only consider dissolution due to the movement of the plume, $C_R = 0$,

B) include the dissolution due to convective mixing, $C_R \neq 0$.

Especially we consider the velocity of the plume tip $v_{tip}$ together with different dissolution rates.

### 6.2.2 Triple Point

The *triple point* is illustrated in the red circle in Figure 6.2. This point is called the triple point because it is surrounded by three regions: mobile $CO_2$, dissolved $CO_2$ and brine. We want to investigate if the plume velocity is dependent on the location of this triple point. That is, if the triple point is located behind the plume tip or if it is located at the tip. Moreover, we find an estimate that says something about when this triple point will catch up with the plume tip for different dissolution rates. In Figure 6.2 a close up of
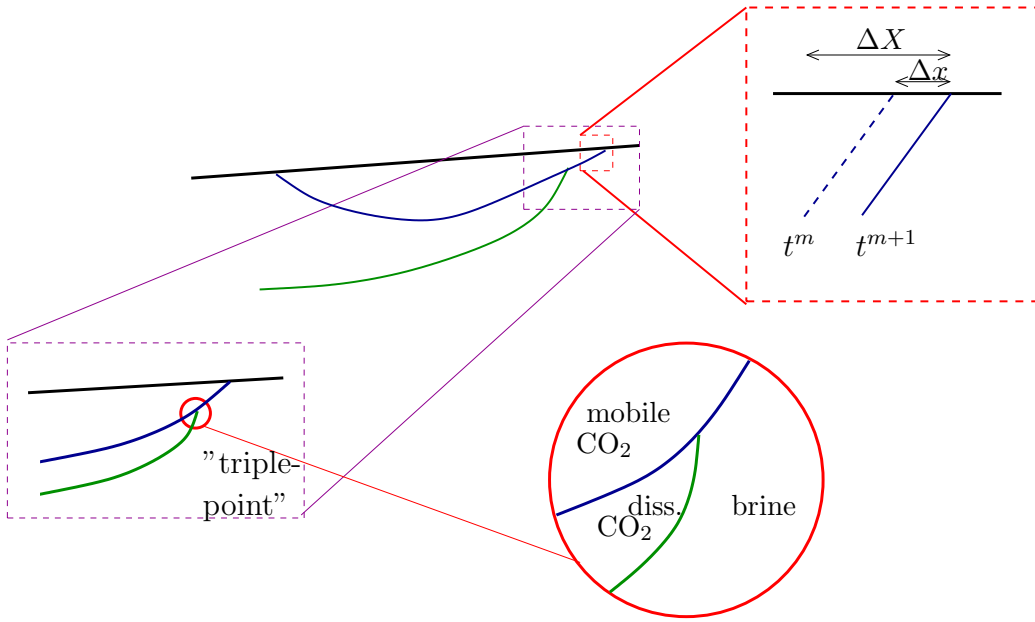


Figure 6.2: *An illustration of what we call the triple point is given in the red circle. In the red frame a close up of the plume tip is illustrated.*

the front tip (rightmost point) of the mobile plume is illustrated in the red frame. We find an expression for the volume change in this region when we not include the effect of convective mixing over a time step $\Delta t$. We take $\Delta x$ to be the spatial transfer of the plume tip over a time $\Delta t$, and $\Delta x$ is given by

$$\Delta x = v_{tip} \, \Delta t,$$

where $v_{tip}$ is the tip velocity. The slope in the plume tip is given by $\partial \zeta_M / \partial x$. The volume change, $\delta V_1$, per time when we not include convective mixing is

$$\delta V_1 \quad = \frac{\Delta x}{\Delta t} \frac{\partial \zeta_M}{\partial x} \Delta X \phi s_{br} = v_{tip} \frac{\partial \zeta_M}{\partial x} \Delta X \phi s_{br}, \qquad \text{unit:} \quad \left[ \frac{m \cdot m}{s} \right]. \quad (6.3)$$

When we include convective mixing the volume change is

$$\delta V_2 \quad = \frac{C_R \Delta X}{\rho_b^{mix} m_b^{c,\text{eq}}}, \qquad \text{unit:} \quad \left[ \frac{m \cdot m}{s} \right], \tag{6.4}$$

where we remember that $\rho_b^{mix} m_b^{c,\text{eq}}$ is the density of dissolved $C0_2$. The ratio between these volume changes can give us a relation between the velocity of the tip point and the velocity of the triple point. When $\delta V_2 > \delta V_1$ the triple point moves faster than the tip point. This means that the volume change $\delta V_2$ can be larger than the volume change $\delta V_1$ as long as the triple point is located behind the tip. When the triple point has caught up with the tip they move with the same velocity and $\delta V_1 = \delta V_2$.

We take the dimensionless number $\beta$ to be the ratio between the volume change $\delta V_1$ and $\delta V_2$,

$$\beta = \frac{\delta V_1}{\delta V_2} \quad = \frac{v_{tip} \frac{\partial \zeta_M}{\partial x} \phi s_{br}}{C_R} \rho_b^{mix} m_b^{c,\text{eq}}. \tag{6.5}$$

To obtain a dissolution region to the right of (ahead of) the mobile plume tip is physically impossible. This means that the triple point never is located in front of the plume tip. When $\delta V_1 = \delta V_2$ we have that the triple point and the tip point is equal, $\beta = 1$.

If we look at the slope $\partial \zeta_M / \partial x$ this means that as long as the triple point is behind the tip point the slope decreases and the angle between $\zeta_M$ and $H$ also decreases. When the triple point catches up with the tip point, the slope $\partial \zeta_M / \partial x$ stops decreasing.

## 6.3   Results

In this Section we present some of the results we have obtained for the model problem presented in Section 6.1. We have studied the plume migration with and without convective mixing and looked at the influence the value of the dissolution rate has on the velocity of the plume tip.

### 6.3.1   Plume Migration

We start by looking at the effect of dissolution the first 5400 years after injection stops when convective mixing not is included. This is the same as saying that the dissolution rate $C_R = 0$. When this is the case, dissolution

of $CO_2$ is due to the movement of the plume. There will still be dissolution as a result of equilibration between mobile $CO_2$ and residual brine as $CO_2$ drains a region with pure brine.

Next, we show the simulations of the plume migration the first 5400 years when we include convective mixing for two different dissolution rates.

1) $C_R = 0\text{kg/m}^2/\text{s}$, in Figure 6.3.

2) $C_R = 3.2 \cdot 10^{-10}$ kg/m$^2$/s $\sim 0.01$kg/m$^2$/year, in Figure 6.4.

3) $C_R = 1.6 \cdot 10^{-9}$ kg/m$^2$/s $\sim 0.05$kg/m$^2$/year, in Figure 6.5.

The dark gray represents the brine, the green represents the dissolved $CO_2$ and the mobile $CO_2$ is white.

In the first case, when $C_R = 0$ we see that a small trail of dissolved $CO_2$ is left behind as the $CO_2$ plume migrates. This dissolution region is created due to the movement of the plume. We see that the dissolved $CO_2$ not is left as a shadow of where the mobile $CO_2$ has migrated, but is forced to lie close to the top of the aquifer. We will return to a discussion around this phenomena.

When we include convective mixing we see that the dissolution region is clearly more visible. The dissolution region starts to develop under the mobile $CO_2$ relatively early for both dissolution rates. However, the dissolution region is thicker and is created earlier for the largest dissolution rate. For the largest dissolution rate we also see that the dissolution region reaches the bottom of the aquifer within the time we are considering.

## Numerical Diffusion

In Figure 6.3, 6.4 and 6.5 we see that we have some diffusion at the back end of the plume. This can not be explained physically since we have chosen $\rho_b^{pure} = \rho_b^{mix}$ and thereby neglected the diffusion term $\partial^2 \zeta_D / \partial x^2$. However, we suspect this to be a result of numerical diffusion. To investigate this we have refined the grid for one dissolution rate for comparison. This refinement showed less diffusion in the back end of the plume. This indicates that the grid chosen not is convergent and that we may have some quantitative differences from a more refined grid. However, the numerical diffusion in the back end of the plume does not give any qualitative differences.
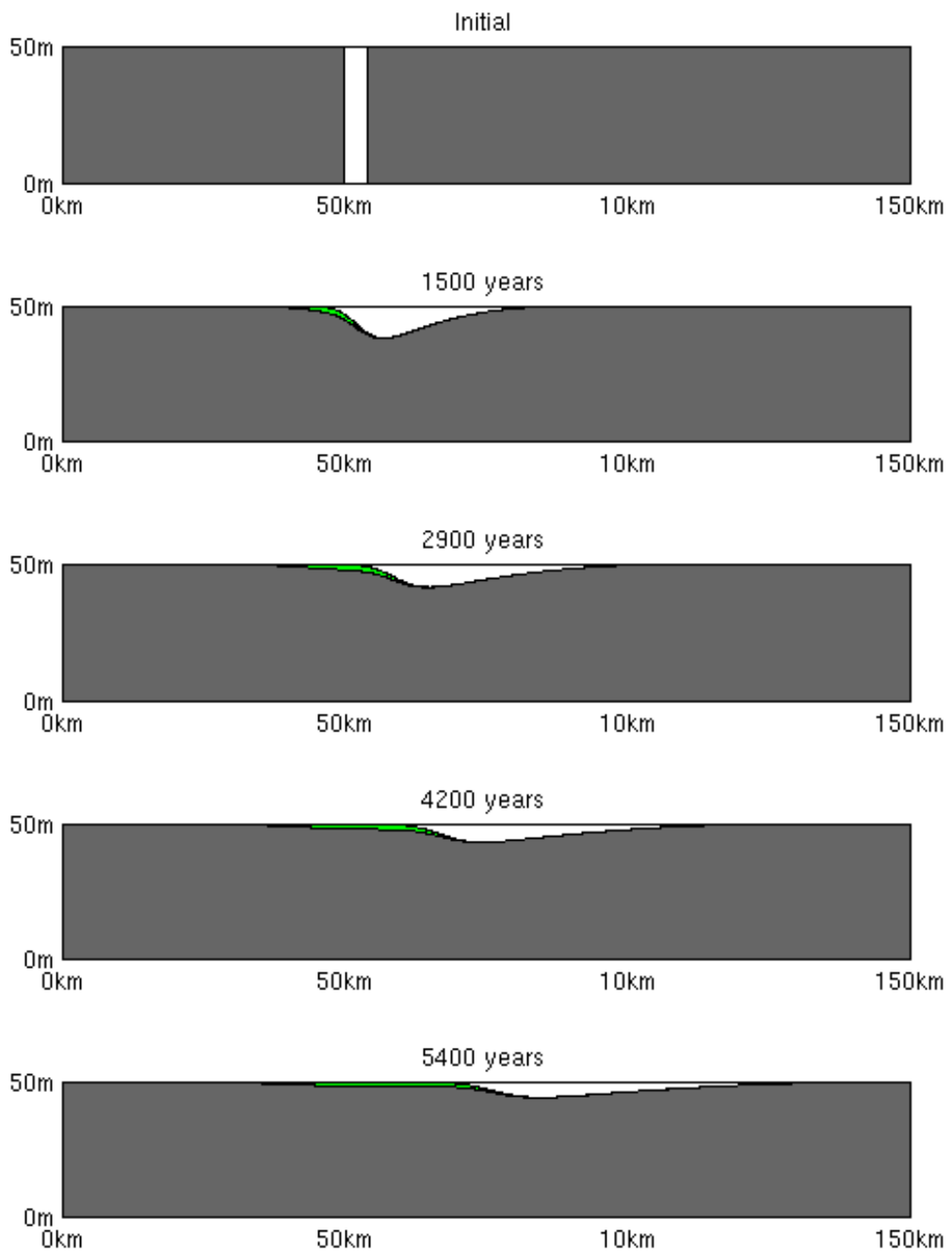
Figure 6.3: *Migration of the $CO_2$ plume the first 5400 years after injection stops. The dark gray represents the brine, the green represents the dissolved $CO_2$ and the mobile $CO_2$ is white. Here is convective mixing not included and $C_R = 0$. We see that after some time it is possible to see the trail of dissolved $CO_2$ behind the mobile $CO_2$.*
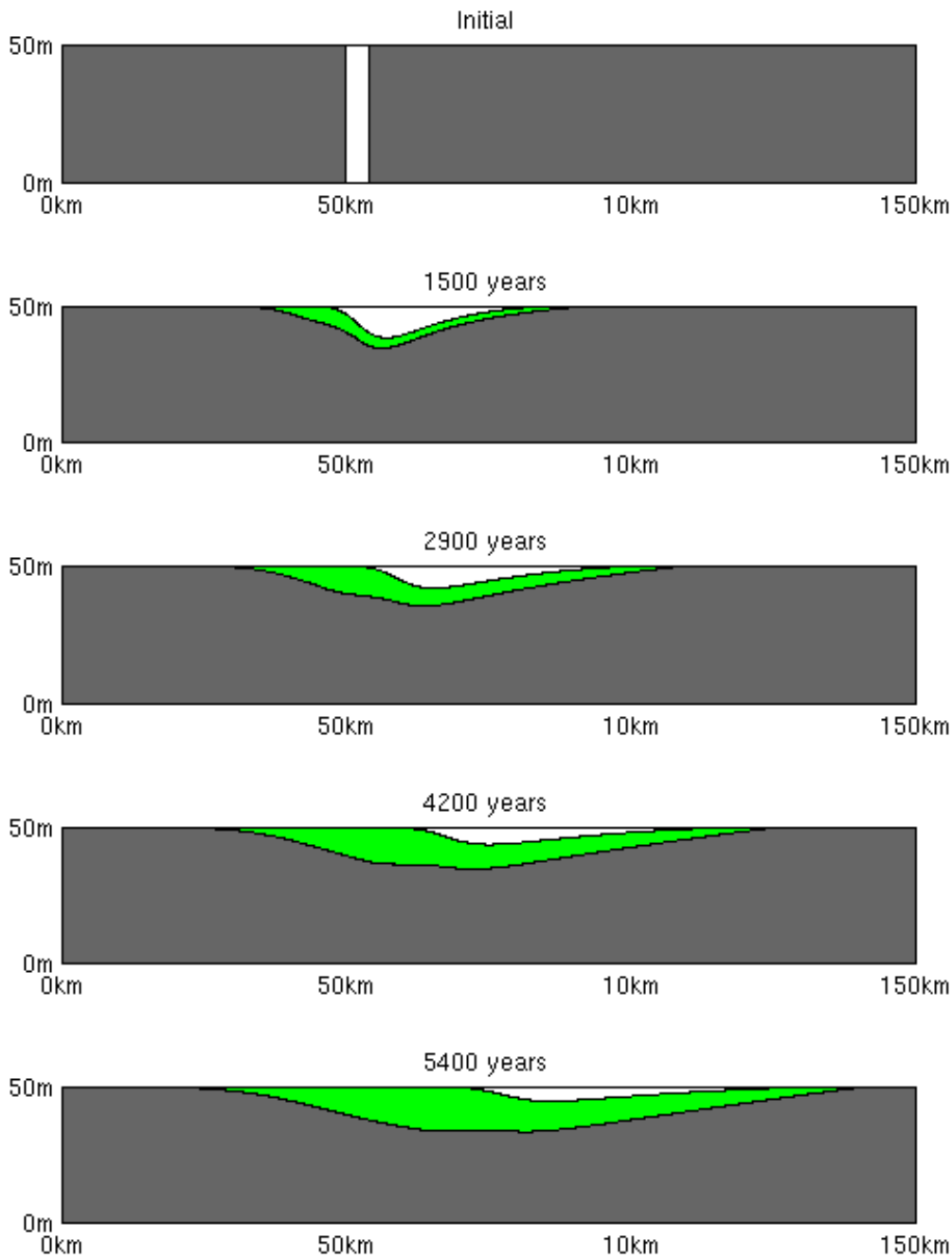
Figure 6.4: *Migration of the $CO_2$ plume the first $5400$ years after injection stops. The dark gray represents the brine, the green represents the dissolved $CO_2$ and the mobile $CO_2$ is white. Here we include convective mixing, and $C_R = 3.2 \cdot 10^{-10}$ $kg/m^2/s$. We see that the trail of dissolved $CO_2$ is more visible than with $C_R = 0$. Also, the dissolution region and the triple point is closer to the plume tip.*
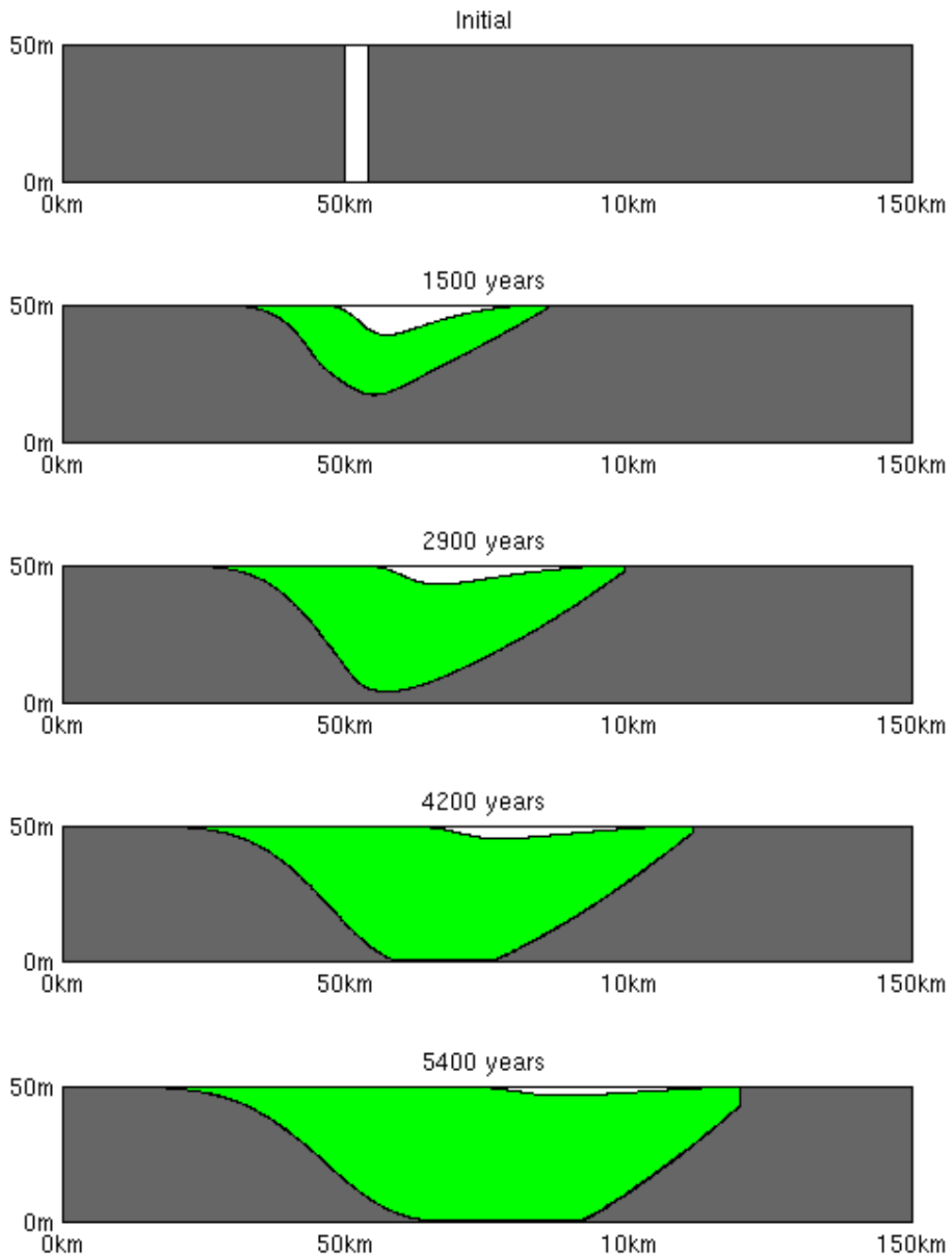
Figure 6.5: *Migration of the $CO_2$ plume the first 5400 years after injection stops. The dark gray represents the brine, the green represents the dissolved $CO_2$ and the mobile $CO_2$ is white. Here we include convective mixing, and*
$C_R =$ $1.6 \cdot 10^{-9}$ *$kg/m^2/s$. We see that the trail of dissolved $CO_2$ is even more visible than with $C_R = 3.2 \cdot 10^{-10}$ $kg/m^2/s$. For this dissolution rate we see that the dissolution region reaches the bottom of the aquifer within the time we are considering.*

### 6.3.2  Dissolution Rate and the Triple Point

As indicated earlier the location of the triple point can be of importance regarding the tip velocity. Here we find some estimates of the dissolution rate when the triple point is located at the tip point. We start by approximating the tip velocity $v_{tip}$ and the slope in the tip $\partial \zeta_M / \partial x$ when convective mixing not is included. From these values we find a limit value $C_{RL}$ for the dissolution rate by setting the dimensionless number $\beta = 1$. When $\beta = 1$ we have that the triple point is located at the tip, and they move with the same. The estimated values for different times are listed in Table 6.3;

| **Time** | $v_{tip}$ | | $C_{RL} \Longleftrightarrow \beta = 1$ |
|---|---|---|---|
| years | m/s | $\dfrac{\partial \zeta_M}{\partial x}$ | kg/m$^2$/s |
| 300 | $1.3 \cdot 10^{-6}$ | 0.042 | $1.6 \cdot 10^{-8}$ |
| 600 | $1.0 \cdot 10^{-6}$ | 0.037 | $1.2 \cdot 10^{-8}$ |
| 900 | $8.9 \cdot 10^{-7}$ | 0.031 | $9.1 \cdot 10^{-9}$ |
| 1500 | $7.6 \cdot 10^{-7}$ | 0.014 | $3.2 \cdot 10^{-9}$ |
| 2200 | $6.7 \cdot 10^{-7}$ | 0.0007 | $1.6 \cdot 10^{-10}$ |
| 2900 | $6.3 \cdot 10^{-7}$ | 0.0002 | $3.2 \cdot 10^{-11}$ |
| 3500 | $6.0 \cdot 10^{-7}$ | 0.0001 | $2.6 \cdot 10^{-11}$ |
| 4200 | $5.7 \cdot 10^{-7}$ | $3.7 \cdot 10^{-5}$ | $7.0 \cdot 10^{-12}$ |
| 4800 | $5.6 \cdot 10^{-7}$ | $2.4 \cdot 10^{-7}$ | $4.3 \cdot 10^{-14}$ |

Table 6.3: *Tip velocities $v_{tip}$ and slopes $\partial \zeta_M / \partial x$ for different times when convective mixing not is included gives estimates on the dissolution rates when the triple point has caught up with the tip point.*

From the numbers in Table 6.3 we choose dissolution rates around the limit vales marked in red for our further discussions on the location of the triple points influence on the tip velocity.

To illustrate the expected effect of the triple points location we look at the plume migration after 2900 years for different dissolution rates, given in Figure 6.6. For the first three dissolution rates the triple point is marked with a red dot, and we see that it is located closer to the tip point for increasing dissolution rates. For the three highest dissolution rates the triple point has caught up with the plume tip. We discuss this further in the next section.
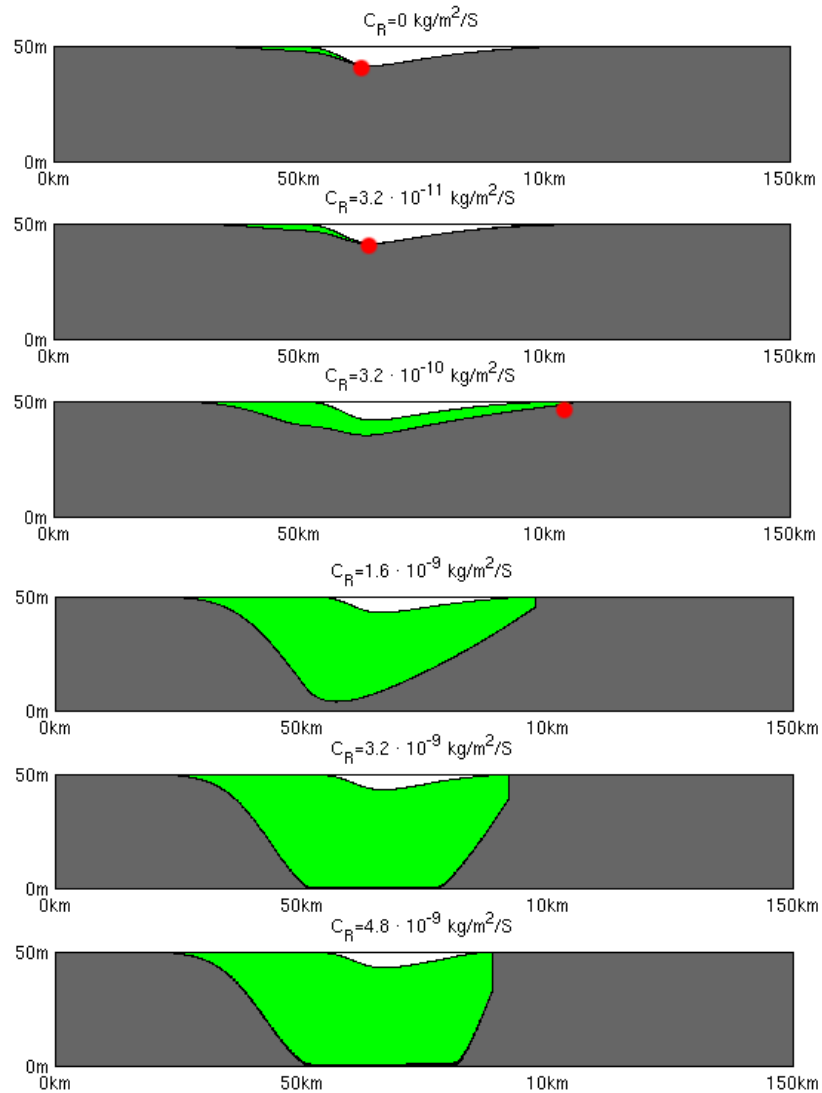
Figure 6.6: *Migration after* 2900 *years with different dissolution rates. Brine is represented in dark gray, dissolved $CO_2$ in green and mobile $CO_2$ in white. The red dots for the three first dissolution rates represents the approximate location of the triple point. For the three last dissolution rates the triple point is located at the tip of the plume, that is: the triple point has caught up with the tip point.*

### 6.3.3 Tip Velocity and Dissolution Rate

For different dissolution rates we investigate the location of the plume tip at different times. We find that the distance from the initial point is dependent on the dissolution rate. This distance decreases for increased dissolution rate

as shown in Figure 6.7. The migrated distance after 5400 years with a dissolution rate $C_R = 0.3 \text{kg/m}^2/\text{year}$ compared to $C_R = 0$ is reduced with almost 50km.

We calculate the tip velocity $v_{tip}$ numerically for 16 different dissolution
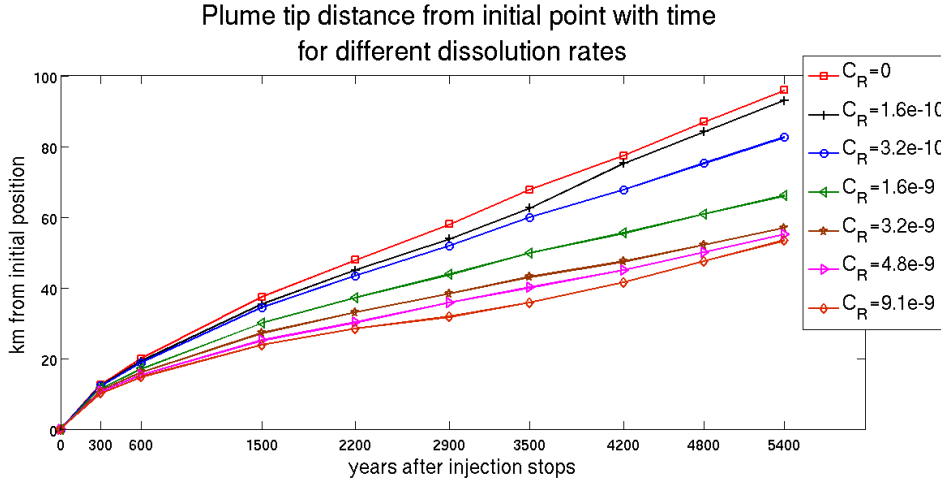


Figure 6.7: *Distance the plume tip has migrated from the initial state with time for different dissolution rates.*

rates, for 4 different times. The dissolution rate is taken to be $C_R \in [0, \, 4.0 \cdot 10^{-9}] \text{ kg/m}^2/\text{s}$, and we look at the tip velocity 300, 600, 1500 and 2900 years after injection stops.

In Figure 6.8 we see the tip velocity after 300, 600, 1500 and 2900 years for increasing dissolution rates. We see that the tip velocity actually is dependent of the dissolution rate. The velocity seems to have *two* characteristic values. One constant tip velocity up to a certain limit dissolution rate $C_{RL}$, and then a velocity dependent of the dissolution rate. This is a observation that not is visible in high numerical simulations by e.g. [30, 28], one reason for this could be the high complexity of the system. However, for our simplified model this phenomena is visible and we can explain this observation with the discussion we had regarding the triple point. For a small dissolution rate ($C_R < C_{RL}$) the triple point is located behind the tip point, and the plume tip migrates with a constant velocity independent of the dissolution rate. When the triple point catches up with the plume tip, the tip velocity changes and becomes a function of the dissolution rate. For later times both the tip velocity and the limit dissolution rate $C_{RL}$ changes, but the trend is the same. Compared to the estimates we found in Table 6.3 the dissolution

rates we looked at seems fairly reasonable. However, we can not conclude anything on the exact limit cases for the dissolution rates.
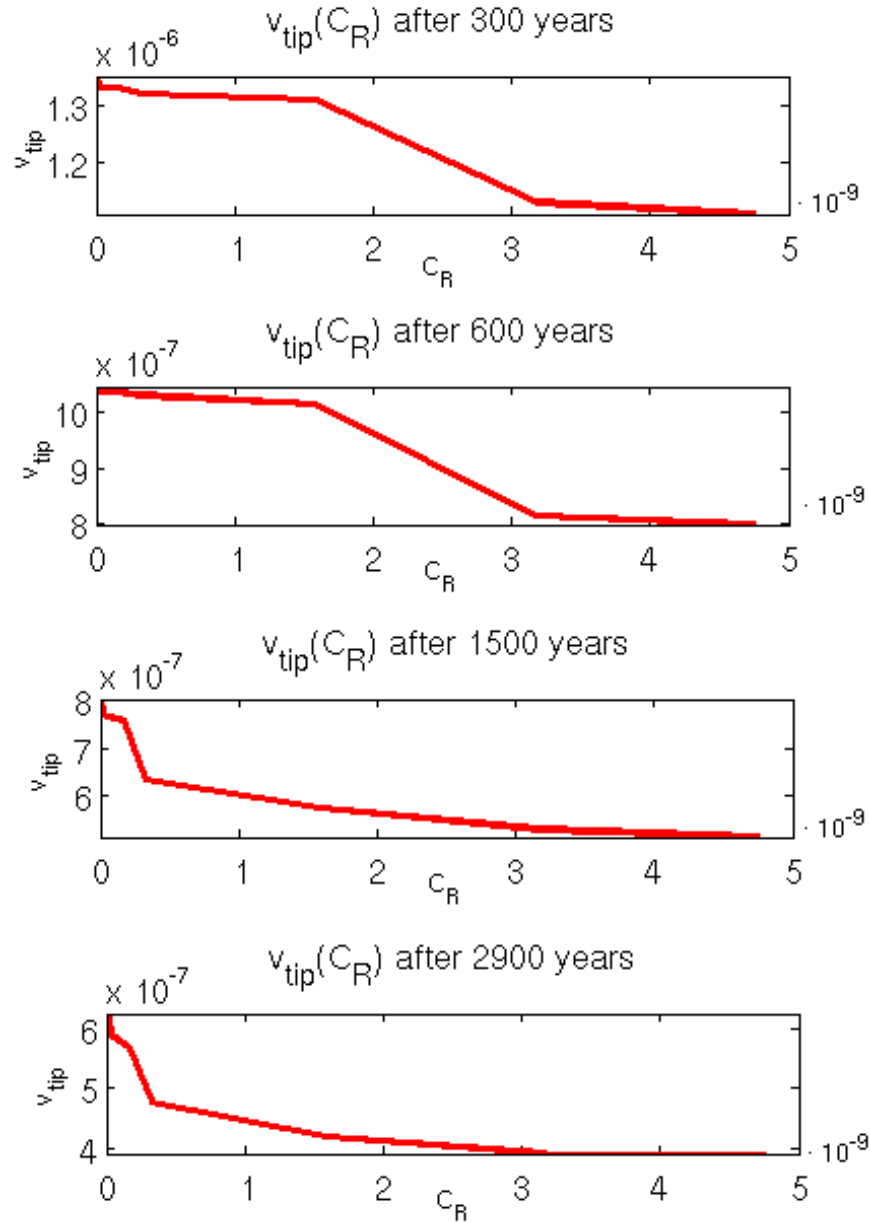


Figure 6.8: *Tip velocity as a function of the dissolution rate $C_R$ for* 300, 600, 1500 *and* 2900 *years. The tip velocity seems to have one characteristic value up to a certain limit dissolution rate, and then a velocity dependent on the dissolution rate for larger dissolution rates.*

### 6.3.4    Trail of Dissolved $CO_2$

In this section we discuss the location of the trail of dissolved $CO_2$ left behind as the mobile $CO_2$ migrates. When convective mixing not is included dissolved $CO_2$ is left behind as $CO_2$ drains pure brine, and one could imagine that the dissolution region is left behind as a shadow of where the mobile $CO_2$ has migrated. However, if we look at the dissolution region after 2900 years in Figure 6.3 and in Figure 6.6 where convective mixing not is included, we see that the dissolution region is located near to the top of the aquifer. This is the opposite of what one might expect. We see that areas previously filled with $CO_2$ now is filled with dissolved $CO_2$ only close to the aquifer top, and brine below the dissolution region.

The situation 2900 years after injection stops when convective mixing not is included is illustrated in Figure 6.9.
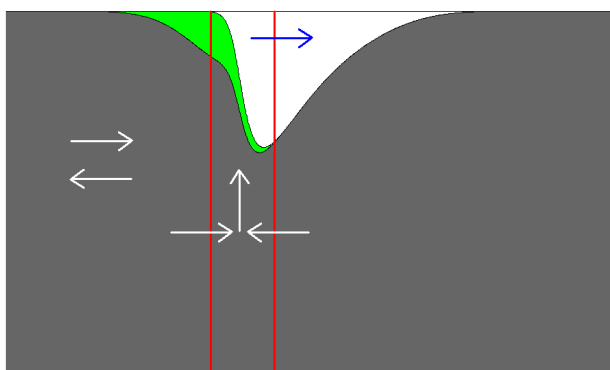


Figure 6.9: 2900 *years after injection stops, with dissolved $CO_2$ located near the top of the aquifer. In the red cross section the brine moves upwards in the vertical direction and acts as a replacement in areas previously filled with mobile $CO_2$. The arrows illustrates the flow directions.*

In the red cross section we have that areas previously filled with $CO_2$ are filled with brine from below as the mobile $CO_2$ plume moves to the right. The white arrow illustrates that the brine moves upwards in the vertical direction. We interpret this to mean that the flow of the wetting phase dominates the dissolution region and brine forces the dissolution region to be close to the top. Behind the red cross section we have that brine only moves in the lateral direction. This means that the situation for the region of dissolved $CO_2$ has stabilized near the top of the aquifer. For increased dissolution rates the phenomena is the same, namely that the brine forces the dissolved $CO_2$ upwards.

# Chapter 7

# Summary and Conclusions

Both the migration process and the trapping processes presented in Chapter 1 are inherently complex. The processes spans multiple spatial and temporal scales. Hence, modeling the problem at scales appropriate for evaluating long term storage of $CO_2$ is computationally expensive.

To simplify the problem it has been common to use sharp interface models with an assumption of vertical equilibrium. Also, to obtain analytical solutions to the problem the effect of dissolution trapping has been neglected. However, it has been shown that dissolution trapping, and especially the effect of convective mixing, can be of great importance when considering $CO_2$ migration.

Analytical solutions to the sharp the interface models discussed in Chapter 3 are limited in the sense that they only include residual trapping. The analytical solutions in [13, 18] show that the time scale associated with the plume migration is so large that the assumption of neglecting dissolution becomes questionable. Therefore, the model presented in Chapter 4 is an improvement in the sense that it includes effects of both direct dissolution and convective mixing. Since we have simplified a very complex process, this framework enables us to model over much larger spatial and temporal scales than would be possible using traditional high resolution numerical models.

We have studied the plume migration with and without the effect of convective mixing and looked at the influence the value of the dissolution rate has on the tip velocity. Physically we have discussed that the location of the triple point (point between region of dissolved $CO_2$, pure brine and mobile $CO_2$) could effect the plume velocity. Our results shows that the value of the dissolution rate has a great impact on the tip velocity. Actually we find

that the tip velocity has two characteristic values. One constant tip velocity up to a certain limit dissolution rate, and then a velocity dependent on the dissolution rate. This has not been shown in high resolution numerical models, and is a phenomena that we actually can explain physically by the location of the triple point. As long as the triple point is located behind the tip of the plume, the tip velocity is independent of the dissolution rate. When the triple point has caught up with the plume tip, the characteristic tip velocity changes. Exactly when the triple point catches up with the tip point is dependent on the dissolution rate. This observation contributes to a better understanding of the dynamics of the plume migration.

# Appendix A

# The Full Flux Expressions

In this appendix the full expression for the spatial derivative of the datum pressure is given. The corresponding component fluxes are also given.

## Pressure Equation

We remember the four different regions:

| | | | | |
|---|---|---|---|---|
| 1 | pure $CO_2$ (mobile), | dissolved $CO_2$ | $H$ | $\{ h_1 = H - \zeta_M$ |
| 2 | pure $CO_2$ (residual), | dissolved $CO_2$ | $\zeta_M$ | $\{ h_2 = \zeta_M - \zeta_R$ |
| 3 | | dissolved $CO_2$ | $\zeta_R$ | $\{ h_3 = \zeta_R - \zeta_D$ |
| 4 | pure brine | | $\zeta_D$ | $\{ h_4 = \zeta_D$ |
| | | | $0$ | |

**Total mass per area for each component:**

$$M^c = \phi \Big[ \ \rho_b^{mix} m_b^{c,\text{eq}} \left( h_3 + (1 - s_{cr}) h_2 + s_{br} h_1 \right) + \tag{A.1}$$
$$\rho_c^{mix} m_c^{c,eq} \left( s_{cr} h_2 + (1 - s_{br}) h_1 \right) \Big],$$

$$M^b = \phi \Big[ \ \rho_b^{mix} m_b^{b,\text{eq}} \left( h_3 + (1 - s_{cr}) h_2 + s_{br} h_1 \right) + \rho_b^{pure} h_4 \tag{A.2}$$
$$\rho_c^{mix} m_c^{b,eq} \left( s_{cr} h_2 + (1 - s_{br}) h_1 \right) \Big].$$

$$M_b^c = \phi \ \ \rho_b^{mix} m_b^{c,\text{eq}} \left( h_3 + (1 - s_{cr}) h_2 + s_{br} h_1 \right) \tag{A.3}$$

**Total flux for each component:**

$$F^c = \rho_b^{mix} m_b^{c,\text{eq}} \left( u_{b3} h_3 + u_{b2} h_2 \right) + \rho_c^{mix} m_c^{c,eq} u_{c1} h_1, \tag{A.4}$$

$$F^b = \rho_b^{mix} m_b^{b,\text{eq}} \left( u_{b3} h_3 + u_{b2} h_2 \right) + \rho_b^{pure} u_{b4} h_4 + \rho_c^{mix} m_c^{b,eq} u_{c1} h_1, \tag{A.5}$$

$$F_b^c = \rho_b^{mix} m_b^{c,\text{eq}} \left( u_{b3} h_3 + u_{b2} h_2 \right). \tag{A.6}$$

**Darcy velocities in each region:**

$$u_{c1} = -k\lambda_{c1} \left( \frac{\partial P}{\partial x} - g \cos\theta \left( \Delta\rho_1 \frac{\partial h_4}{\partial x} - \Delta\rho_2 \frac{\partial h_1}{\partial x} \right) - g\rho_c^{mix} \sin\theta \right),$$

$$u_{b2} = -k\lambda_{b2} \left( \frac{\partial P}{\partial x} - g \cos\theta \Delta\rho_1 \frac{\partial h_4}{\partial x} - g\rho_b^{mix} \sin\theta \right),$$

$$u_{b3} = -k\lambda_{b3} \left( \frac{\partial P}{\partial x} - g \cos\theta \Delta\rho_1 \frac{\partial h_4}{\partial x} - g\rho_b^{mix} \sin\theta \right),$$

$$u_{b4} = -k\lambda_{b4} \left( \frac{\partial P}{\partial x} - g\rho_b^{pure} \sin\theta \right),$$

$$\text{where} \qquad \Delta\rho_1 = \rho_b^{pure} - \rho_b^{mix}, \qquad\qquad \Delta\rho_2 = \rho_b^{mix} - \rho_c^{mix}.$$

**Mass conservation equations:**

$$\frac{\partial M^c}{\partial t} + \frac{\partial F^c}{\partial x} = 0 \tag{A.7}$$

$$\frac{\partial M^b}{\partial t} + \frac{\partial F^b}{\partial x} = 0 \tag{A.8}$$

$$\frac{\partial M_b^c}{\partial t} + \frac{\partial F_b^c}{\partial x} = C_R, \tag{A.9}$$

**Pressure Equation:**

$$A_1 \left( \frac{\partial M^b}{\partial t} + \frac{\partial F^b}{\partial x} \right) + A_2 \left( \frac{\partial M^c}{\partial t} + \frac{\partial F^c}{\partial x} \right) + A_3 \left( \frac{\partial M_b^c}{\partial t} + \frac{\partial F_b^c}{\partial x} \right) = A_3 C_R,$$

$$\Updownarrow \qquad \text{(A.10)}$$

$$\frac{\partial}{\partial x} \left( A_1 F^b + A_2 F^c + A_3 F_b^c \right) = A_3 C_R,$$

where:

$$A_1 = \frac{1}{\rho_b^{pure}},$$

$$A_2 = \frac{1}{\rho_c^{mix} m_c^{c,\text{eq}}} - \frac{m_c^{b,\text{eq}}}{\rho_b^{pure} m_c^{c,\text{eq}}},$$

$$A_3 = \frac{1}{\rho_b^{mix} m_b^{c,\text{eq}}} - \frac{1}{\rho_c^{mix} m_c^{c,\text{eq}}} + \frac{m_c^{b,\text{eq}}}{\rho_b^{pure} m_c^{c,\text{eq}}} - \frac{m_b^{b,\text{eq}}}{\rho_b^{pure} m_b^{c,\text{eq}}}.$$

**Isolated expression for the datum pressure from (A.10):**

$$\boxed{\frac{\partial P}{\partial x} = p_1(\boldsymbol{h}, x) + p_2(\boldsymbol{h})\frac{\partial h_4}{\partial x} + p_3(\boldsymbol{h})\frac{\partial h_1}{\partial x},} \qquad \text{(A.11)}$$

where $\boldsymbol{h} = [\, h_1 \; h_2 \; h_3 \; h_4 \,]$,

$$p_1 = \frac{1}{C_1 + C_2 + C_3}\left( g\sin\theta \left(\rho_c^{mix} C_1 + \rho_b^{pure} C_3 + \rho_b^{mix} C_2\right) - \frac{A_3 C_R (x - \tilde{x})}{k} \right),$$

$$p_2 = \frac{1}{C_1 + C_2 + C_3} g\cos\theta \Delta\rho_1 (C_1 + C_2),$$

$$p_3 = -\frac{1}{C_1 + C_2 + C_3} g\cos\theta \Delta\rho_2 C_1,$$

where we have defined

$$C_1 = \lambda_{c1} h_1 (A_1 \rho_c^{mix} m_c^{b,\text{eq}} + A_2 \rho_c^{mix} m_c^{c,\text{eq}}),$$

$$C_2 = (\lambda_{b3} h_3 + \lambda_{b_2} h_2)(A_1 \rho_b^{mix} m_b^{b,\text{eq}} + (A_2 + A_3)\rho_b^{mix} m_b^{c,\text{eq}}),$$

$$C_3 = \lambda_{b4} h_4 A_1.$$

# Expressions for the Component Fluxes

We insert the expression for the datum pressure (A.11) to obtain the full expressions for the different fluxes (A.4, A.5, A.6).

**Total flux for the CO$_2$ component:**

$$\boxed{F^c = f_1^c(\boldsymbol{h}, x) + f_2^c(\boldsymbol{h})\frac{\partial h_4}{\partial x} + f_3^c(\boldsymbol{h})\frac{\partial h_1}{\partial x},} \tag{A.12}$$

where

$$f_1^c = -k\Big( \rho_b^{mix}m_b^{c,\text{eq}}(\lambda_{b3}h_3 + \lambda_{b2}h_2)\left[p_1 - g\rho_b^{mix}\sin\theta\right] +$$
$$\rho_c^{mix}m_c^{c,\text{eq}}\lambda_{c1}h_1\left[p_1 - g\rho_c^{mix}\sin\theta\right] \Big),$$

$$f_2^c = -k\Big(\rho_b^{mix}m_b^{c,\text{eq}}(\lambda_{b3}h_3 + \lambda_{b2}h_2) + \rho_c^{mix}m_c^{c,\text{eq}}\lambda_{c1}h_1\Big)\left[p_2 - g\Delta\rho_1\cos\theta\right],$$

$$f_3^c = -k\Big(\rho_b^{mix}m_b^{c,\text{eq}}(\lambda_{b3}h_3 + \lambda_{b2}h_2)p_3 + \rho_c^{mix}m_c^{c,\text{eq}}\lambda_1 h_1\left[p_3 + g\Delta\rho_2\cos\theta\right]\Big).$$

**Total flux for the brine component:**

$$\boxed{F^b = f_1^b(\boldsymbol{h}, x) + f_2^b(\boldsymbol{h})\frac{\partial h_4}{\partial x} + f_3^b(\boldsymbol{h})\frac{\partial h_1}{\partial x},} \tag{A.13}$$

where

$$f_1^b = -k\Big( \rho_b^{mix}m_b^{b,\text{eq}}(\lambda_{b3}h_3 + \lambda_{b2}h_2)\left[p_1 - g\rho_b^{mix}\sin\theta\right] +$$
$$\rho_c^{mix}m_c^{b,\text{eq}}\lambda_{c1}h_1\left[p_1 - g\rho_c^{mix}\sin\theta\right] + \rho_b^{pure}\lambda_{b4}h_4[p_1 - g\rho_b^{pure}\sin\theta]\Big),$$

$$f_2^b = -k\Big( \Big(\rho_b^{mix}m_b^{b,\text{eq}}(\lambda_{b3}h_3 + \lambda_{b2}h_2) + \rho_c^{mix}m_c^{b,\text{eq}}\lambda_{c1}h_1\Big)\left[p_2 - g\Delta\rho_1\cos\theta\right] +$$
$$\rho_b^{pure}\lambda_{b4}h_4 p_2\Big),$$

$$f_3^b = -k\Big( \rho_b^{mix}m_b^{b,\text{eq}}(\lambda_{b3}h_3 + \lambda_{b2}h_2)p_3 + \rho_c^{mix}m_c^{b,\text{eq}}\lambda_1 h_1\left[p_3 + g\Delta\rho_2\cos\theta\right] +$$
$$\rho_b^{pure}\lambda_{b4}h_4 p_3\Big).$$

**Total flux for the dissolved CO$_2$:**

$$\boxed{F_b^c = f_{b1}^c(\boldsymbol{h}, x) + f_{b2}^c(\boldsymbol{h})\frac{\partial h_4}{\partial x} + f_{b3}^c(\boldsymbol{h})\frac{\partial h_1}{\partial x},} \tag{A.14}$$

where

$$f_{b1}^c = -k\rho_b^{mix}(\lambda_{b3}h_3 + \lambda_{b2}h_2)\left[p_1 - g\rho_b^{mix}\sin\theta\right],$$

$$f_{b2}^c = -k\rho_b^{mix}(\lambda_{b3}h_3 + \lambda_{b2}h_2)\left[p_2 - g\Delta\rho_1\cos\theta\right],$$

$$f_{b3}^c = -k\rho_b^{mix}(\lambda_{b3}h_3 + \lambda_{b2}h_2)p_3.$$

# Appendix B

# Nomenclature

| Symbol | Description | Unit |
|---|---|---|
| $\phi$ | (Effective) porosity | - |
| $\rho$ | Desity | $kg/m^3$ |
| $\mu$ | Viscosity | $kg/ms$ |
| $c$ | Compressibility | - |
| $V$ | Volume | $m^3$ |
| $p$ | Pressure | $kg/ms^2$ |
| $s_\alpha$ | Saturation of phase $\alpha$ | - |
| $s_{\alpha r}$ | Residual saturation of phase $\alpha$ | - |
| $m_\alpha^i$ | Mass fraction of component $i$ in phase $\alpha$ | - |
| $\rho_\alpha^{mix}$ | Mix density phase $\alpha$ | $kg/m^3$ |
| $\rho_b \alpha^{pure}$ | Pure density phase $\alpha$ | $kg/m^3$ |
| $\mathbf{u}$ | Darcy velocity / Volumetric flux | $m/s$ |
| $\mathbf{k}$ | Permebility | $m^2$ |
| $g$ | Accelaration due to gravity | $m/s^2$ |
| $k_{r\alpha}$ | Relative permeability phase $\alpha$ | - |
| $\lambda_\alpha$ | Mobility for phase $\alpha$ | - |
| $s_{wn}$ | Normalized water saturation | - |
| $P_c$ | Capillary pressure | $kg/ms^2$ |
| $\mathbf{F}$ | Flux | $kg/m^2s$ |
| $q$ | Source / sink term | - |
| $C$ | Concentration | $kg/m^3$ |
| $D$ | Diffusion coeffcient | - |
| $\theta$ | Dip angle | - |
| $T$ | Teperature | $^\circ$ C |
| $H$ | Thickness of the aquifer | m |
| $S_\alpha$ | Vertically integrated saturation | - |
| $\Lambda_\alpha$ | Vertically integrated mobility | - |
| $C_R$ | Mass production rate of dissolved $CO_2$ per time | $kg/m^2/s$ |
| $\zeta_M$ | Interface for mobile $CO_2$ | - |
| $\zeta_R$ | Interface for residual $CO_2$ | - |
| $\zeta_D$ | Interface for dissolved $CO_2$ | - |

# Bibliography

[1] IPCC Fourth Assessment Report: Climate Change 2007. *Report of the Intergovernmental Panel on Climate Change,IPCC*, 2007.

[2] I. Aavatsmark. *Bevarelsesmetoder for hyperbolske differensialligninger.* University of Bergen, Bergen, 2004.

[3] S. Bachu. Screening and ranking of sedimentary basins for sequestration of $CO_2$ in geological media in response to climate change. *Environmental Geology*, 44(3):277–289, 2003.

[4] S. Bachu, D. Bonijoly, J. Bradshaw, R. Burruss, S. Holloway, N. P. Christensen, and O. M. Mathiassen. $CO_2$ storage capacity estimation: Methodology and gaps. *International Journal of Greenhouse Gas Control*, 1(4):430–443, 2007.

[5] S. Bachu, W. D. Gunter, and E. H. Perkins. Aquifer disposal of $CO_2$: Hydrodynamic and mineral trapping. *Energy Conversion and Management*, 35(4):269–279, 1994.

[6] J. Bear. *Dynamics of fluid in porous media.* American Elsevier, New York, 1972.

[7] J. Bradshaw, S. Bachu, D. Bonijoly, R. Burruss, S. Holloway, N. P. Christensen, and O. M. Mathiassen. $CO_2$ storage capacity estimation: issues and development of standards. *International Journal of Greenhouse Gas Control*, 1(1):62–68, 2007.

[8] R. H. Brooks and A. T. Corey. Hydraulic properties of porous media. *Hydraulic Paper*, 1(3), 1964.

[9] H. K. Dahle, G. T. Eigestad, J. M. Nordbotten, and K. Pruess. A model-oriented benchmark problem for $co_2$ storage. *Princeton-Bergen Seminar on Carbon Storage*, 2009.

[10] J. Ennis-King and L. Paterson. Role of convective mixing in the long-term storage of carbon dioxide in deep saline formations. *SPE Journal*, 10(3):349–356, 2005.

[11] R. A. Freeze and J. A. Cherry. *Groundwater*. Prentice Hall, Englewood Cliffs, New Jersey, 1979.

[12] Gasda, S. and Nordbotten, J. M. and Celia, M. A. Vertically-Averaged Approaches for $CO_2$ injection. *Water Resources Researh*, submitted, 2010.

[13] M. A Hesse, F. M Orr, and H. A Tchelepi. Gravity currents with residual trapping. *Journal of Fluid Mechanics*, 611:35–60, 2008.

[14] C. Holger. *Models for Non-Isothermal Compositional Gas-Liquid Flow and Transport in Porous Media*. PhD thesis, University of Stuttgart, 2007.

[15] S. Holloway and D. Savage. The potential for aquifer disposal of carbon dioxide in the UK. *Energy Conversion and Management*, 34(9-11):925–932, 1993.

[16] H. E. Huppert and A. W. Woods. Gravity-driven flows in porous layers. *Journal of Fluid Mechanics*, 292:55–69, 1995.

[17] F. P. Incropera and D. P. DeWitt. *Introduction to heat transfer*. John Wiley & Sons New York, 1996.

[18] R. Juanes, C.W. MacMinn, and M.L. Szulczewski. The Footprint of the CO 2 Plume during Carbon Dioxide Storage in Saline Aquifers: Storage Efficiency for Capillary Trapping at the Basin Scale. *Transport in Porous Media*, 82(1):19–30, 2009.

[19] Andreas Kopp. *Evaluation of $CO_2$ Injection Processes in Geological Formations for Site Screening*. PhD thesis, University of Stuttgar, 2009.

[20] L. W. Lake. *Enhanced oil recovery*. Englewood Cliffs, 1989.

[21] R. J. LeVeque. *Numerical Methods for Conservation Laws*. Birkhäuser, 1992.

[22] E. Lindeberg and D. Wessel-Berg. Vertical convection in an aquifer column under a gas cap of $CO_2$. *Energy Conversion and Management, 38*, 229(234):229–324, 1997.

[23] S. Lyle, H. E. Huppert, M. Hallworth, M. Bickle, and A. Chadwick. Axisymmetric gravity currents in a porous medium. *Journal of Fluid Mechanics*, 543:293–302, 2005.

[24] J. M. Nordbotten and M. A. Celia. Similarity solutions for fluid injection into confined aquifers. *Journal of Fluid Mechanics*, 561:307–327, 2006.

[25] J. M. Nordbotten and M. A. Celia. *Geological Storage of $CO_2$: Modeling Approaches for Large-Scale Simulation.* For publication, Wiley InterScience, 2010.

[26] J.M. Nordbotten and H.K. Dahle. Impact of the capillary fringe in vertically integrated models for $CO_2$ storage. *In Press, Water Resources Research*, 2010.

[27] S. Pacala and R. Socolow. Stabilization wedges: solving the climate problem for the next 50 years with current technologies. *Science*, 305(5686):968–972, 2004.

[28] G. S. H. Pau, J. B. Bell, K. Pruess, A. S. Almgren, M. J. Lijewski, and K. Zhang. High Resolution Simulation and Characterization of Density-Driven Flow in CO2 Storage in Saline Aquifers. *Advances in Water Resources*, 33(-1):443–455, 2010.

[29] Ø. Pettersen. Grunnkurs i reservoarmekanikk. *Lecture notes, Department of Mathematicks, University of Bergen*, 1990.

[30] K. Pruess. Numerical simulation experiments on the long-term evolution of a $CO_2$ plume under a sloping caprock. *Report, Lawrence Berkeley National Laboratory*, 2010.

[31] A. Riaz, M. Hesse, HA Tchelepi, and FM Orr. Onset of convection in a gravitationally unstable diffusive boundary layer in porous media. *Journal of Fluid Mechanics*, 548:87–111, 2006.

[32] W. F. Smith and J. Hashemi. *Foundations of materials science and engineering.* McGraw-Hill, New York, 1993.

[33] R. Span and W. Wagner. A new equation of state for carbon dioxide covering the fluid region from the triple-point temperature to 1100 K at pressures up to 800 MPa. *Journal of Physical and Chemical Reference Data*, 25(6):1509–1596, 1996.